Organic & Polymer-based Lithium Ion Batteries

A Thesis

Presented to

the Faculty of the Department of Mechanical Engineering

University of Houston

In Partial Fulfillment

of the Requirements for the Degree

Master of Science

in Mechanical Engineering

by

Sridhar Reddy Appanapalli

August 2012

Organic & Polymer-based Lithium Ion Batteries

Sridhar Reddy Appanapalli

Approved:

Chair of the Committee
Haleh Ardebili, Assistant Professor,
Mechanical Engineering

Committee Members:

Jagannatha R.Rao, Associate Professor,
Mechanical Engineering

Allan J.Jacobson, Professor
Department of Chemistry

Suresh K. Khator, Associate Dean,
Cullen College of Engineering

Pradeep Sharma, Professor and
Chair, Mechanical Engineering

ACKNOWLEDGMENTS

I would like to thank my advisor, Professor Haleh Ardebili for believing in me and graciously accepting me into her research group and also for her patience, guidance, support, invaluable suggestions and help in making this thesis possible.

I also acknowledge Mejdi Kammoun and Eric Wood for their help in making a flexible battery. I would like to thank Syed Haque for his help with SEI analysis. I would like to thank Qin Li for his help in making battery components. I would like to thank Mengying Yuan for taking great pictures of my samples and lab equipment. I would like to thank Narayan Das Khatri and Mufaddal for their help in spin coating and scanning electron microscopy respectively. I would like to thank the Max Plank Institute for supplying us with the polymer material.

I also want to thank my committee members Dr. Jagannatha R.Rao and Dr. Allan J. Jacobson for their insightful comments and suggestions. I am forever grateful to my family and friends for their help in every form towards my thesis. I dedicate this thesis to my parents.

Organic & Polymer-based Lithium Ion Batteries

An Abstract

Of a

A Thesis

Presented to

the Faculty of the Department of Mechanical Engineering

University of Houston

In Partial Fulfillment

of the Requirements for the Degree

Master of Science

in Mechanical Engineering

by

Sridhar Reddy Appanapalli

August 2012

Abstract

Polymer-based electrode and electrolyte components can pave the way for safe and flexible Lithium ion batteries. A total plastic battery requires an electrolyte layer to be sandwiched between thin polymer layers. Polymer components offer significant advantages including enhanced safety, stability and thin film manufacturability.

In this study, we investigate the fabrication, assembly and characterization of organic and polymer based Lithium ion batteries. Specifically, we used PEO (Polyethylene oxide) for electrolyte. We used polymers PVBPT and PTMA for electrodes and utilized organic fillers and binders to improve the electrical conductivity of the polymer. These polymers work as electrode by releasing or collecting electron from Li through their radical polymer chain during charge and discharge. A flexible battery was prepared using conventional electrode and polymer electrolyte. Conventional coin cells with standard electrode and electrolyte materials were also assembled and tested for comparison. Cyclic voltammetry, electrochemical impedance spectroscopy and SEM are included.

Table of Contents

List of Figures

List of Tables

Chapter 1: INTRODUCTION

1.1 Energy Storage:

Energy storage is accomplished by specific techniques and devices that store various forms of energy to perform useful operation at a later time. Currently, the entire world is faced with several energy issues such as eventual depletion of earth's fossil fuels, environmental concerns and global warming. Some of the solutions to energy crisis can be cleaner fossil fuel consumption, renewable energy sources, efficient energy consumption products and efficient and advanced energy storage technologies [24].

Energy storage is as important as energy harvesting. We can judge this fact from our current technology trends. Apart from the electrical energy for domestic and industrial purposes that is produced and consumed instantaneously during high peak hours, most of the energy generated has to be stored and retrieved at a later time. Hence much attention is being directed towards regarding efficient and advanced energy storage technologies.

Various types of energy storage options are illustrated in figure 1-1[24]. Batteries are classified under electrochemical energy storage. The invention of the battery can be dated back to Alessandro Volta in 1800s who constructed the first battery by stacking Zn and Cu plates in an aqueous solution separated by a paper. A battery is a device that produces electricity from a chemical reaction. A cell consists of a negative electrode; an

electrolyte, which conducts ions; a separator, also an ion conductor; and a positive electrode. The electrolyte may be aqueous (composed of water) or nonaqueous (not composed of water), in liquid, paste, or solid form.

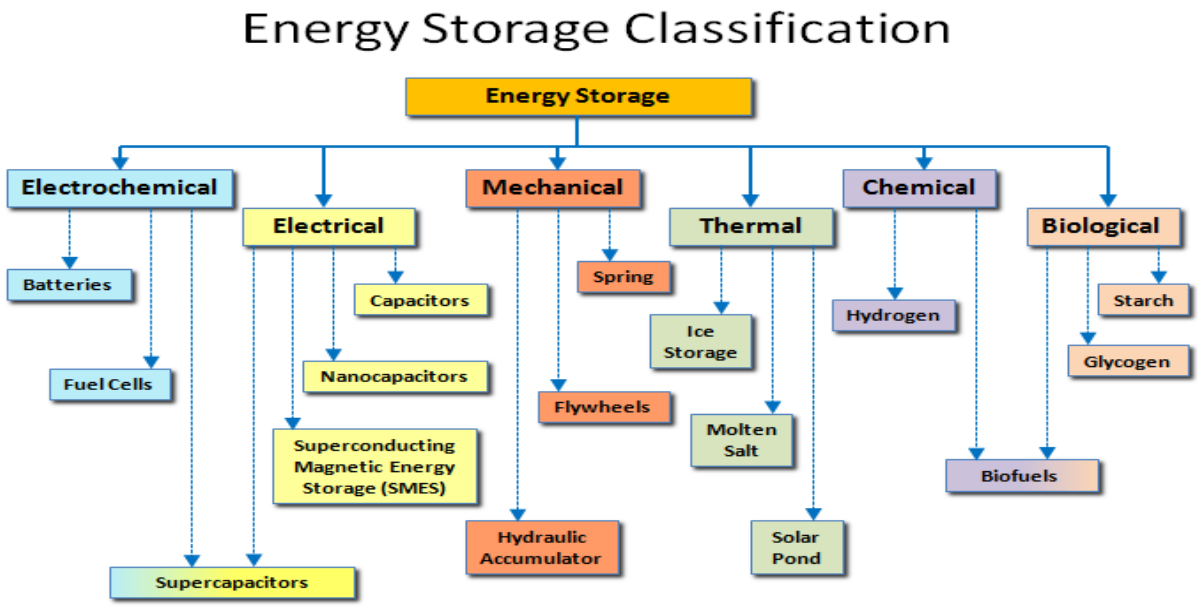

Figure 1-1. Schematic representation of various energy storage options.

When the cell is connected to an external load, or a device which is powered, the negative electrode supplies a current of electrons that flow through the load and are accepted by the positive electrode. When the external load is removed the reaction ceases. A primary battery is one that can convert its chemicals into electricity only once and then must be discarded. A secondary battery has electrodes that can be reconstituted by passing electricity back through it; also called a storage or rechargeable battery and can be reused many times.

Rechargeable batteries come in many different shapes and sizes, ranging anything from a button cell to megawatt systems. Batteries are being widely used as power sources ranging from automotive applications to portable electronic devices like cellular phones, laptop computers, digital cameras, music players etc., because of their high-energy density and long life [19, 20].

Every secondary cell constitutes a positive electrode and a negative electrode separated by electrolyte and separator. The separator is used mainly to prevent short circuit, more importantly should allow transfer of ions but not electrons, electrolyte types can range from solid to liquid. During charging, the positive active material is oxidized, producing electrons, and the negative material is reduced, consuming electrons. These electrons constitute the current flow in the external circuit. The electrolyte serves as a simple buffer for internal ion flow between the electrodes.

1.2 Lithium Ion Battery

The discovery of Lithium and Lithium transition-metal oxides as negative and positive electrodes for a secondary cell has revolutionized the energy storage option and made batteries ubiquitous and, of course, a general household term. Lithium is the lightest metal and has one of the highest standard reduction potentials. The combination of these two characteristics gives the element particularly favorable energy content, with a theoretical specific capacity of 3860 Ah kg^{-1} in comparison with 820 Ah kg^{-1} for zinc and 260 Ah kg^{-1}. Therefore, Lithium ion batteries offer high energy density compared to other devices as shown in figure 1-2 (a) [24]. Since the standard reduction

potential of Lithium is more negative than 3.0 V, the metal is thermodynamically unstable in protic solvents such as water but stable in organic solvents [20].

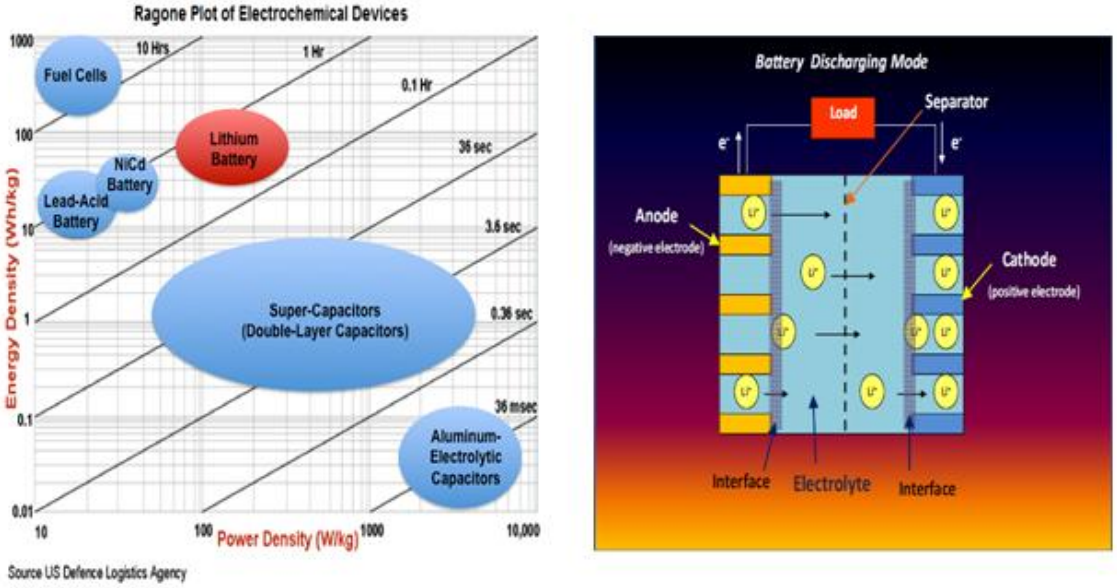

(a) (b)

Figure 1-2. Ragone plot (a) and schematic representation (b) of charge/discharge mechanism in a Lithium ion or rocking chair battery.

During charging mode the Lithium in the cathode (positive electrode) gets oxidized and the Lithium ion becomes deintercalated, travels through the electrolyte to intercalate at the anode (negative electrode) and the exactly reverse process occurs during discharging mode at the cathode. The main problem arises when the Lithium ions do not occupy the interstitial lattice space inside the metal but start becoming attached at the electrode interface. If this process continues they grow like a bridge and finally reach the opposite electrode causing short circuiting thereby likely to cause an explosion. This is termed as dendrite growth. Lithium metal can be deposited at current

collector and locations other than inside the electrode where the deposition is actually desired.

To overcome the safety issues associated with Lithium metal several alternative options were researched. The alternative options were the electrolyte and electrode. Layered or three-dimensional-type transition-metal oxides doped with Lithium ion have been chosen to function as positive electrodes. The general representation of the Lithium transition-metal oxides is LixMyXz (M – transition metal, X-oxygen and y, z – number of atoms). The best transition metal oxides must have the following characteristics: should permit a large amount of Lithium to be inserted/extracted, to maximize cell capacity Lithium insertion/extraction process must be reversible, and should have both good electronic conductivity and good Lithium ion conductivity, must be chemically stable without undergoing any reaction with the electrolyte over the entire range of Lithium insertion/extraction and the redox energy of the cathode material must lie within the band gap of the electrolyte to prevent unwanted oxidation or reduction of the electrolyte. Typical Lithium transition metal oxides are $LiMO_2$ (M=V, Cr, Co and Ni) and LiM_2O_4 (M=Ti, V, Mn).

The discovery of the highly reversible, low voltage Li intercalation–deintercalation process in carbonaceous material led to the replacement of a negative electrode and eventually $C/LiCoO_2$ are realized as having a potential exceeding 3.6 V and gravimetric energy densities as high as 120–150 Wh kg^{-1} is found in most of today's high-performance portable electronic devices [22, 24]. The second option involved replacing liquid electrolytes by Solid Polymer Electrolyte (SPE). Polymer electrolyte usually

contains a polymer matrix, a salt (mostly Li based) with/without liquid solvent to cause swelling. The following are the advantages of SPE: it can act as both an electrolyte and separator, it eliminates dendrite growth and conforms to the varying volume of electrodes during recycling, it is less reactive and thermodynamically more stable towards Lithium and has enhanced safety and shape flexibility. The following are the challenges being faced by researchers to realize SPE in a Lithium ion battery: it has poor ionic conductivity compared to liquid electrolytes and high impedance due to solid-solid interface.

The Lithium transition-metal oxide cathode constitutes the main part of a Lithium ion battery hence determining the battery's energy density and capacity along with the problems associated with it. The Lithium transition-metal oxide is charged/discharged in accordance with deintercalation/ intercalation of the Lithium ions and oxidation/reduction of the transition-metal ions. This causes the structural change of the cathode and hence reduces cycle life and capacity [19-22]. The increased use of transition metal compounds as cathode active material in Lithium ion batteries will ultimately lead to an increase in material cost. In addition, the current cathode materials based on cobalt are toxic and recycling problems are not yet solved. New materials based on organic compounds are therefore an attractive alternative. Conducting radical polymers are a promising alternative to Lithium transition-metal oxides as a candidate for cathode active material from the viewpoints of high power density and environmental friendliness [1, 2, 6, 15, 16, and 18].

1.3 Organic Lithium Ion Battery

1.3.1 Radical Polymer

A polymer which has unpaired electrons is called a radical polymer. Conducting radical polymers are promising alternatives to Lithium transition-metal oxides as cathode active materials from the viewpoints of high power density, realization of flexible batteries and environmental friendliness. The radical polymers are unstable in their natural state and have tendency to become stable through redox reactions with other molecules thus making them suitable as electrode materials [1, 2, 18].

Radical polymers show reversible redox electrochemical reactions in aprotic solutions and hence are an alternative active material for Lithium metal oxides. For example, the highest theoretical capacity of the nitroxyl radical polymers is 147mAhg^{-1} which is comparable to the practical specific capacity of LiCoO2 (140mAh g^{-1}) [2, 18, 22, 23] and the theoretical specific capacity of PVBPT is 86mAhg^{-1}. A battery composed of the radical polymer electrode is called Organic Radical Battery (ORB) [2, 18].

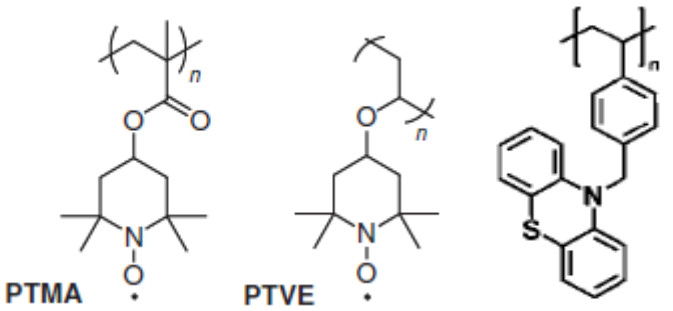

Figure 1-3. Molecular structures of PTMA, PVTE and PVBPT.

Radical polymers consist of two main components: a radical pendant (2,2,6,6, tetramethylpiperidine-1-oxyl (TEMPO), phenothiazine etc.) and a backbone polymer (polymethacrylate, polyvinyl ether, polyvinyl benzyl etc.). When the above radical pendants are polymerized with the respective backbone polymers result in the following radical polymers:

PTMA – poly (2, 2, 6, 6-tetramethylpiperidine-4-yl-1-oxylmethacrylate)

PVTE – poly (2, 2, 6, 6-tetramethylpiperidine-4-yl-1-oxyl vinyl ether)

PVBPT – poly 10-(4-vinylbenzyl)-10H-phenothiazine [1, 2, 17].

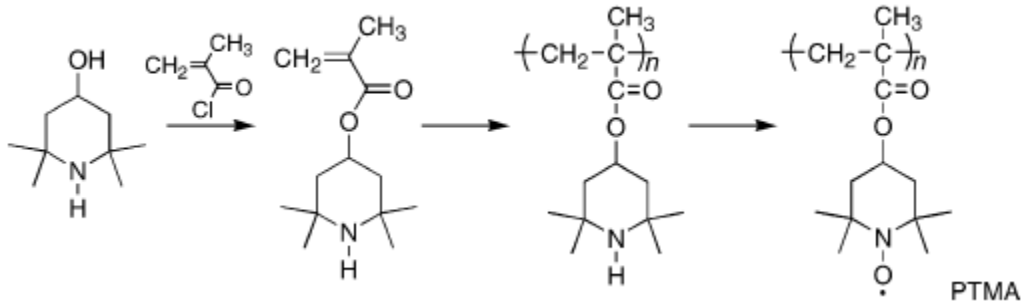

Figure 1-4. Polymerisation of TEMPO to PTMA.

Figure 1-4 shows the sequence of the products formed and the chemicals used in polymerizing TEMPO to PTMA [1]. 2,2,6,6-tetramethylpiperidine methacrylate is prepared by polymerizing 2,2,6,6-tetramethyl-4-piperidinol and methacryloyl chloride 2,2´-azobisisobutyronitrile as the radical initiator. This precursor polymer when treated with 3-chloroperoxybenzoic acid yields PTMA.

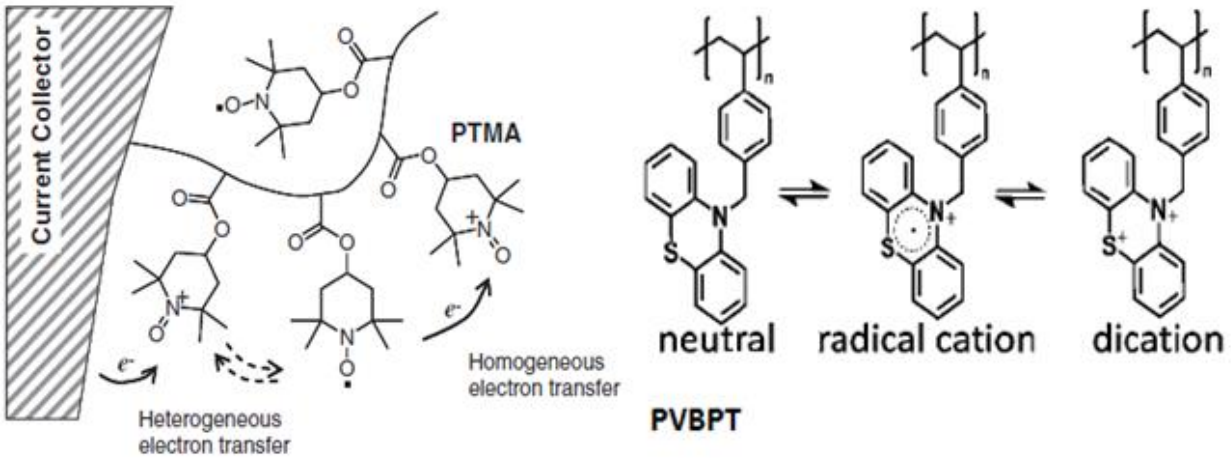

Figure 1-5. Electron transfer profile in a radical polymer electrode.

The electron transfer process in radical polymers is thought to have two electron transfer steps. The first step is the heterogeneous electron transfer from a current collector to the radical component. The second step is homogeneous electron transfer among the radical components. In the homogeneous step, electron transfers are apparently driven by the concentration gradient through an electron self-exchange reaction between neighboring radicals. Phenothiazine has two unpaired electrons, one on a nitrogen atom and the other on a sulphur atom as opposed to TEMPO which has only one electron. Hence PVBPT offers a possibility of two oxidation (charging) and reduction (discharging) peaks unlike PTMA, PVTE or any other radical polymers [2, 7, 17].

1.3.2 Organic Electrode

Radical polymers do not exhibit sufficient electrical conductivity for battery operation and thus must be mixed with generally high percentage of conductive filler

materials like carbon. The carbon acts as a bridge between the polymer radicals and the current collector forming a continuous support for electronic conduction [3]. The polymer and carbon are blended together in a solvent along with a binder to ensure good connection between the polymer and carbon particles. This mixture is finally coated on to a current collector like aluminum foil by spin coating or doctor blade coating and finally dried resulting in an electrode. If Lithium transition metal oxides as cathode and Li metal as anode are replaced by radical polymers and graphite, then the conventional Li ion battery can be called as organic Li ion battery or Organic Radical Battery [1-18].

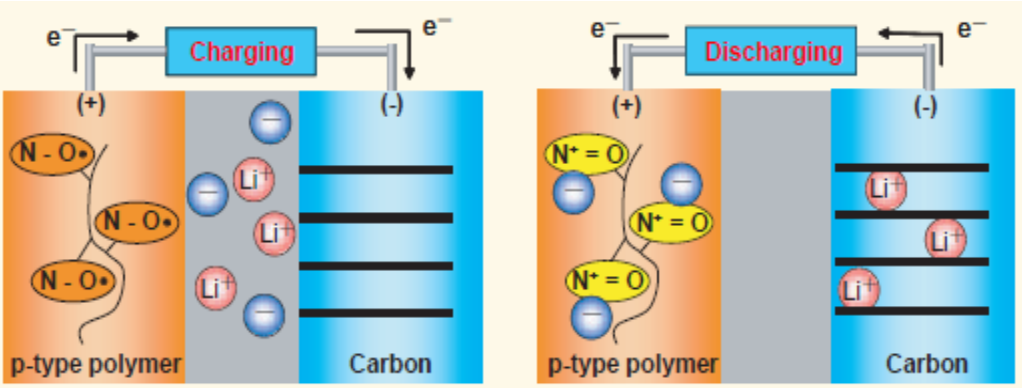

Figure 1-6. A Lithium ion battery based on a radical polymer cathode.

Figure 1-6 shows the charging and discharging mechanism of an organic radical battery where a p-type nitroxide radical polymer forms a cathode. During the charging process, the radical polymer gets oxidized by losing its unpaired electrons, and during discharging, the nitroxide radical is regenerated by reduction [7, 8, 18].

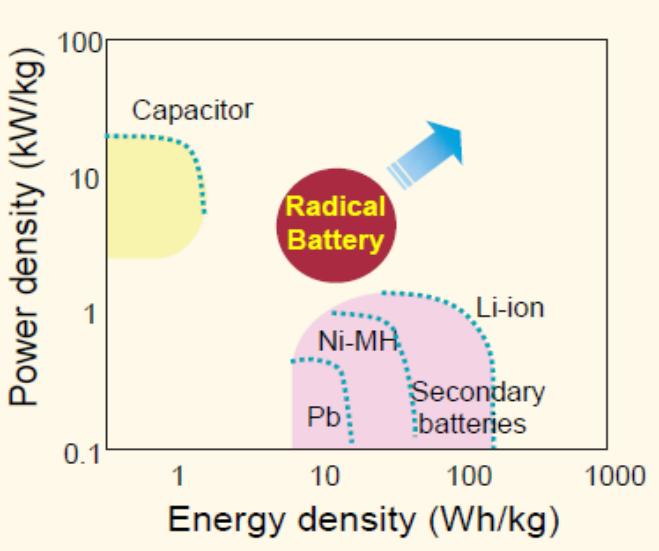

Figure 1-7. Battery performance of the organic radical battery based on the PTMA cathode relative to conventional charge storage devices.

We can observe from figure 1-7 that the performance of ORB involves high power density as high as capacitors and energy density as high as secondary batteries. But the energy density is still lower than Li-ion batteries and has to be improved in this area [18].

1.4 Electrode/Electrolyte Interface Issues

Solid Electrolyte Interphase (SEI) is formed by the reduction of electrolyte solution due to thermodynamic instability of the electrolyte solution towards Lithium ion. SEI is formed between active materials close to the electrode and electrolyte. The SEI layer consists of organic components, from reduction of solvents in electrolyte, and inorganic components, from reduction of salts in electrolyte. A model of the SEI layer

with organic and inorganic contents arranged separately has been proposed. According to the model, electrode is followed by active material and inorganic portion of SEI, which is followed by the organic portion of SEI followed by electrolyte. In the cathode, mostly inorganic components of SEI are present on the edges and cross sections, and organic components are present on the surface.

For a conventional Lithium ion battery using Lithium transition metals oxides as a cathode and Li metal as an anode (half-cell), during charged state two kinds of semicircles along with a slanted line are observed. The two resistances are attributed to surface film resistance and charge transfer resistance. The Warburg impedance (line) is attributed to the impedance associated with the diffusion of Lithium ions. It has been found that the interface forms as soon as the charging starts and at an increase of approximately 0.002V and becomes stabilized in very few cycles. During the impedance analysis, the interface is considered as a resistor and a capacitor connected in parallel. The property of a good interface is that it should allow only ions to pass through it and should act as an insulator for electronic conduction. Hence it is considered as protective layer. Irreversible charge loss, rate capability, cyclability and safety are highly dependent on the quality of SEI. Hence understanding the actual nature and composition of SEI is deemed as important [25-35].

Chapter II: EXPERIMENTAL

Figure 2-1 represents a glove box which actually enables to prepare coin cells in an inert (argon) atmosphere containing typically 0.5ppm of moisture. All the battery components (including a crimping machine) always stay inside the glove box. It consists of two ante chambers (large and small) which enable the process of transferring objects inside and outside the glove box.

Figure 2-1. Glove box.

The coin cells are sealed using the crimping machine as shown in Figure 2-2. Once the whole components are inside of the coin cell casings they are assembled in order, the battery (negative casing) is placed on the holder with the flat surface. Then, the rotating handle is rotated completely in a clockwise manner until the machine locks completely. Then the side handle is moved up and down until the desired pressure is reached and the rotating handle is turned in anti clockwise manner to unlock the crimping machine and the obtained sealed cell is taken out for electrochemical characterization.

Figure 2-2. Compact hydraulic crimping machine.

2.1 Preparation of conventional Lithium Ion coin cells and required components

The following components have been utilized for coin cell construction in the order of their stacking:

1) Positive casing – Diam.20×3.2t mm (304 stainless steel-CR2032, MTI Co)

   Cathode – Diam.15×0.1mm (Aluminium foil as current collector, single side coated by $LiCoO_2$, MTI Co)

2) Separator – Diam.19×0.025t mm (Polyethene, MTI Co)
3) Anode – Diam.15.6×0.25t mm (Lithium chip, MTI Co)
4) Electrolyte – 1ml (1 mol/L $LiPF_6$ in EC+DMC+DEC; 1:1:1 in volume, MTI Co)
5) Spacer – Diam.15.4×0.2 mm (304 stainless steel, MTI Co)
6) Spring (304 stainless steel, MTI Co)
7) Negative Casing – Diam.20×3.2t mm (304 stainless steel-CR2032, MTI Co)

The cathode and separator are baked in vacuum oven for 2 hours at 120°C and 60°C (respectively, to make sure they are totally moisture free) then they are steeped in the electrolyte in two different containers for over 12 hours before being used in the battery to check their stability in the electrolyte. Once all the components have been stacked in order between the positive and negative casings, the coin cell is crimped using crimping machine. The cell assembly was performed under argon atmosphere in a glove box with moisture content less than 1ppm.

Figure 2-3 shows the complete setup of the PGSTAT connected to the computer to be operated through Nova software. Different electrode probes (in varying colors like black, blue, red and green) along with coin cell holder can be observed in the picture. The counter electrode used in this PGSTAT is Lithium.

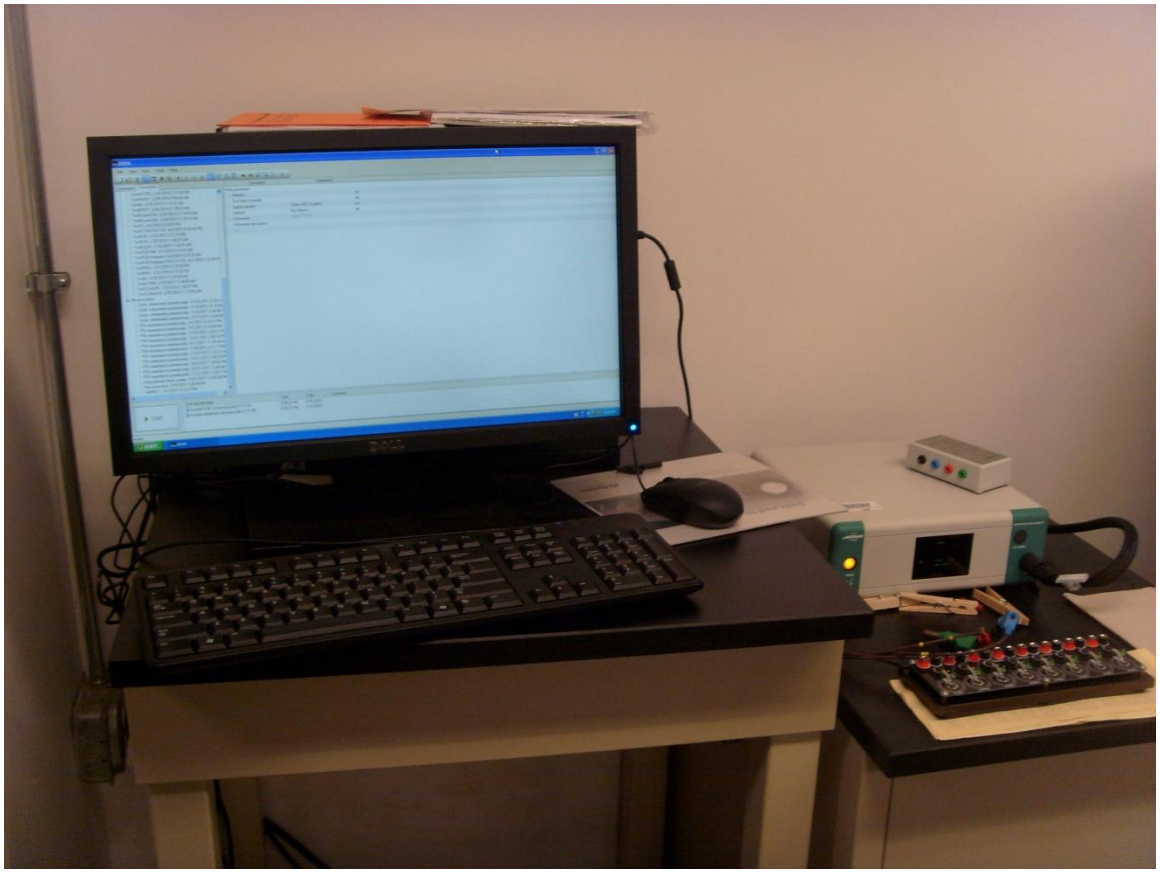

Figure 2-3. PGSTAT/Metrohm Autolab.

2.1.1 Electrochemical measurements performed

The charge–discharge and cycling properties of the cell were evaluated between 3.4 and 4.4 V at different current densities using a PGSTAT (Metrohm Autolab) at room

temperature. Cyclic voltammetry (CV) measurement of the cell was conducted at a scan rate of 10µV/s between 2.7 and 4.4.

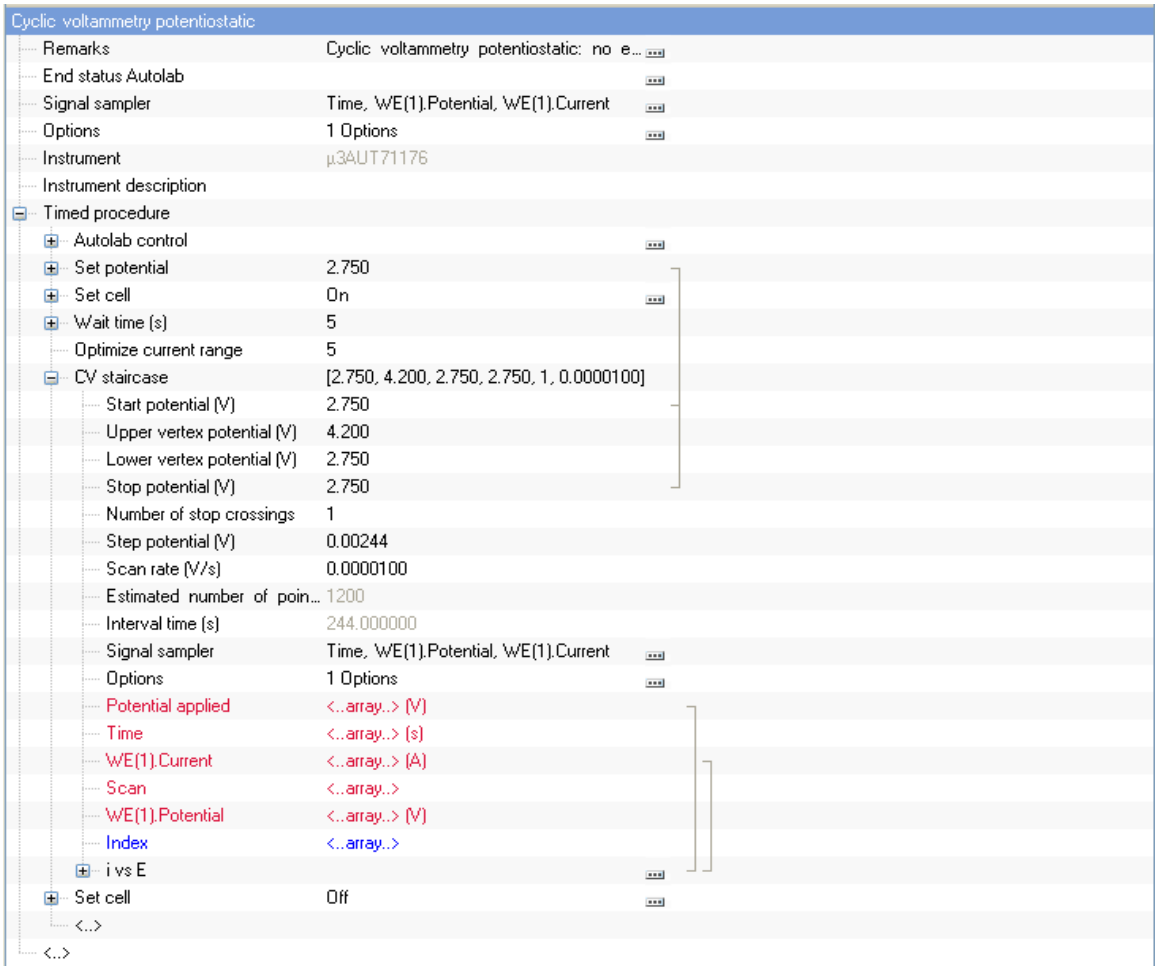

Figure 2-4. Cyclic voltammetry potentostatic procedure in Nova, Autolab.

Figure 2-4 represents the steps and parameters involved in running a CV experiment using Autolab. The CV staircase command has the following parameters:

- Start potential (V): defines the start potential, in Volts. The start potential value can be located outside of the scan range defined by the lower and upper vertices.

- Upper vertex potential (V): defines the upper vertex potential, in Volts. The upper vertex potential must be higher than the lower vertex potential.
- Lower vertex potential (V): defines the lower vertex potential, in Volts. The lower vertex potential must be lower than the upper vertex potential.
- Stop potential: defines the stop potential, in Volts. The stop potential value must be located within the scan range defined by the upper and lower vertices.
- Number of stop crossings: defines the number that the scan should cross the stop potential value in order to stop the measurement.
- Step potential (V): defines the length of the potential step used in the CV staircase command, in Volts. The step potential can be positive or negative. With a positive step, the scan starts from the start potential towards the upper vertex potential. With a negative step, the scan direction is reversed.
- Scan rate (V/s): defines the scan rate, in Volts per second.
- Signal sampler: defines the specific sampler used during the CV staircase. By default, Time, Potential applied and WE(1).Current are measured, but additional electrochemical signals can be added to the sampler. The other signals could be like calculating charge or capacity.

Electrochemical Impedance Spectroscopy (EIS) was done using the Metrohm Autolab at room temperature. The EIS measurements were performed with 10 mV perturbation amplitude in the range from 100 kHz to 10 mHz in automatic sweep mode from high to low frequencies. Data acquisition and analysis were done using Nova 1.6 software.

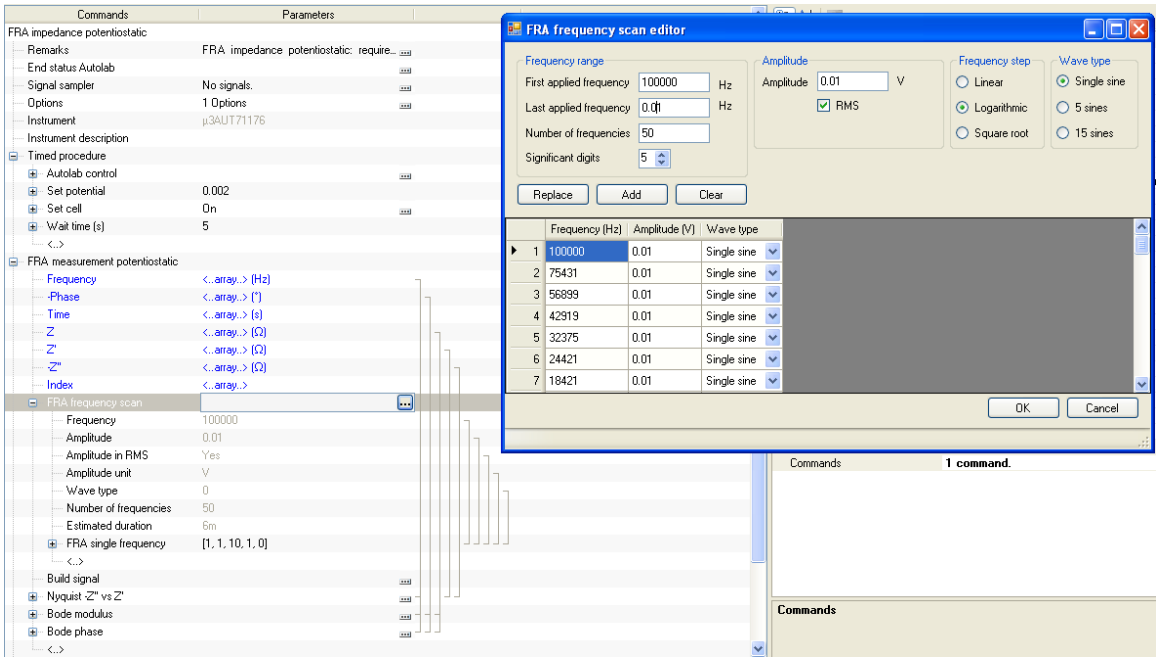

Figure 2-5. FRA Impedance potentiostatic procedure in Nova, Autolab

Figure 2-5 represents the procedure window in Nova for performing impedance analysis across the coin cell. The set potential should always be maintained at 0.002V to avoid short-circuiting across the cell.

2.2 Preparation of Polymer based Cathode

The pure polymer is coated on to a substrate or current collector, using a spin coater shown in figure 2-6. The grey colored circular holder inside the steel casing is called a "vacuum chuck" onto which the substrate is placed. The vacuum chuck has a hole at the center which is connected to a vacuum pump so as to enable the substrate to be in position while it is revolving at higher rpm. The problem with the vacuum chuck and substrate is that the aluminum foil, used as substrate here is very thin. It has a thickness of 15µm. Hence it is placed directly onto the chuck and is getting sucked into the hole

because of the applied vacuum. To avoid this Al foil is spread onto a microscope cover glass having dimensions of 22mmx22mmx5mm. An excess amount of a solution is placed on the substrate using a syringe. Then the plate is spun at required speeds usually in the range of 500 to 1000 rpm and for a time period of 30 to 60 seconds.

Figure 2-6. Spin coater.

The doctor blade is mainly used to cast composite polymer on to a substrate as it is not possible to coat a uniform composite solution using spin coater. The doctor blade has a width of 150mm, slurry capacity of 60ml and can coat with a thickness ranging from 0 to 9000µm. The current collector is spread on to the glass plate and the doctor blade is set on the substrate. To apply the desired thickness, the blade clearance can be set vertically by adjusting the two micrometer-heads. The two micrometer-heads are rotated to make the underside of the blade and the two sides on the same level. The two micrometer-heads are adjusted to get desired blade clearance, which is the film thickness. The two ends of the blade are held (in hand) after pouring the thick viscous

solution onto the substrate near blade, then, moved to and fro to get a uniform coating. Once the coating is obtained the instrument is cleaned with a solution and the spring must be loosened.

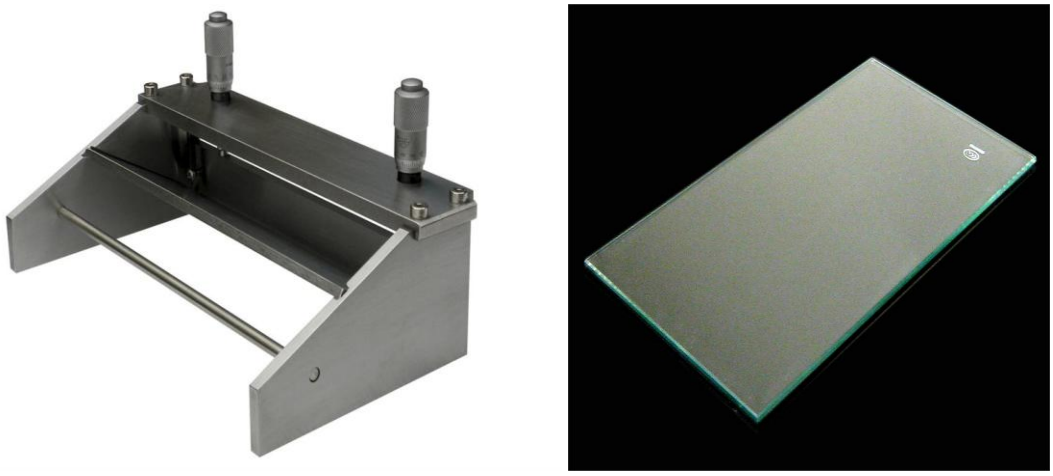

(a) (b)

Figure 2-7. Film casting doctor blade and tempered glass plate.

2.2.1 Pure PTMA based cathode

30mg of the radical polymer, poly(2,2,6,6-tetramethylpiperidinyloxy-4-yl methacrylate) (PTMA), is mixed in 6ml of NMP (N-Methyl-2-pyrrolidone) which is already being stirred on a magnetic stirrer (RT 15 power IKAMAG) and left for stirring for an hour to get well mixed solution. The resulting solution was spin coated on aluminum (which also serves as current collector) at a speed of 1000rpm for 30 seconds. The coated aluminum foil was dried at 70°C for 12 hours to get the cathode film. Circular discs with a diameter 15mm and mass ~0.5mg were cut from the film and used as

cathodes in cells for performing the electrochemical characterizations. The thickness achieved for this cathode was 20µm.

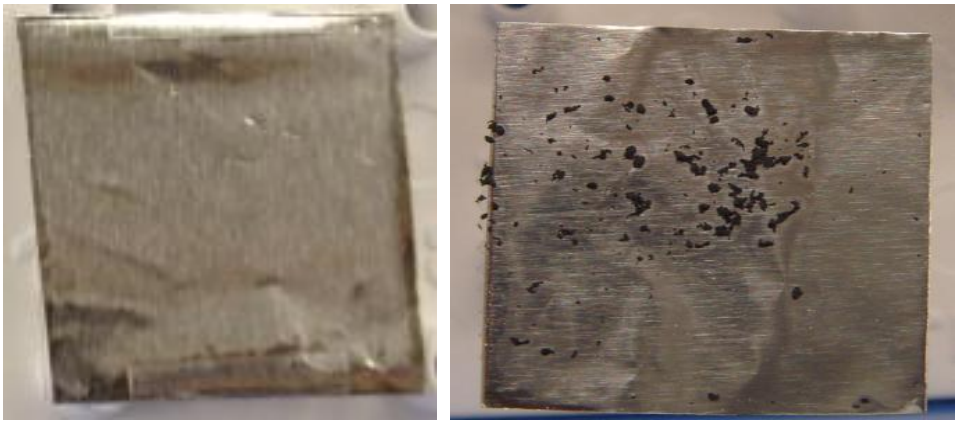

(a) (b)

Figure 2-8. Pure PTMA(a) and composite PTMA(b) obtained from spin coating

It can be observed in Figure 2-8(b) that the filler is not coated uniformly as well as the polymer. The reason is that the filler weighs high when compared to the pure polymer; and when the substrate is spun at higher speeds, the filler flies away from the surface because of the experienced centrifugal force. Hence it can be concluded that composite polymers should not be spin coated.

2.2.2 Composite PTMA based cathode

The cathode was prepared by blending 10mg of the active material PTMA, 70mg of conductive carbon (Acetylene Black), and 20mg of binder PVdF (Polyvinylidene diflouride) in 6ml of NMP and stirred together to form a uniform solution. The resulting

solution was dried in a vacuum oven at 204°C until a desirable viscosity was achieved for casting. The final viscous solution was cast onto an aluminum foil (which also serves as current collector) with a doctor blade having a clearance of 200µm and dried at 70°C for 12 hours to get the cathode film. Circular discs with a diameter 15mm and mass ~1.3mg were cut from the film and used as cathodes in cells for performing the electrochemical characterizations. The thickness achieved for this cathode was 50µm.

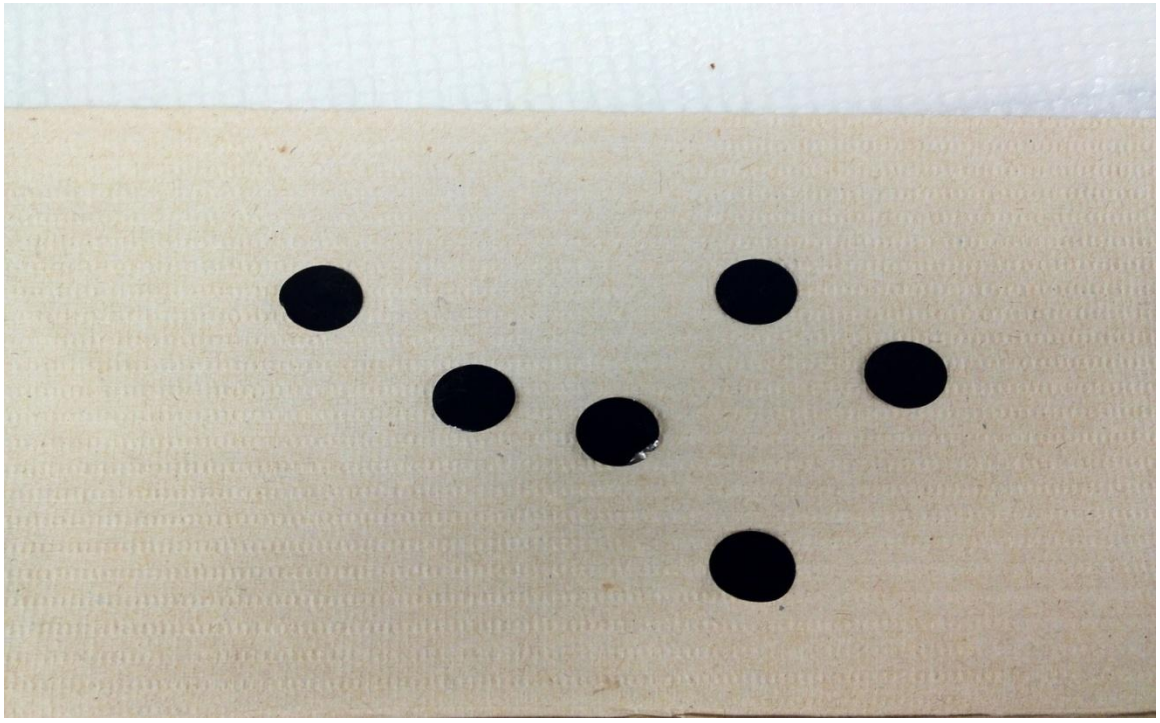

Figure 2-9. Composite PTMA cathodes of 15mm diameter.

Figure 2-9 represents composite PTMA cathodes obtained after doctor blade coating and drying in vacuum ovens. From the picture of black discs we can observe that the black carbon filler has been used in high percentage (70%) compared to the polymer.

2.2.3 Electrochemical measurements performed

Finally, a coin cell was prepared (as mentioned in the section 2.1 'Preparation of Conventional Lithium Ion Coin Cells') by stacking either pure or composite PTMA based cathode and the rest of the components as mentioned in the above list. The charge–discharge and cycling properties of the cell were evaluated between 0 and 4 V at different current densities using a PGSTAT (Metrohm Autolab) at room temperature. Cyclic Voltammetry (CV) measurement of the cell was conducted at a scan rate of 10mV/s between 0 and 4.

Electrochemical Impedance Spectroscopy (EIS) was done using the Metrohm Autolab at room temperature. The EIS measurements were performed with 10 mV perturbation amplitude in the range from 100 kHz to 10 mHz in automatic sweep mode from high to low frequencies. Data acquisition and analysis were done using Nova 1.6 software.

2.2.4 Pure PVBPT based cathode

30mg of the radical polymer poly(10-(4-vinylbenzyl)-10H-phenothiazine) (PVBPT) is mixed in 6ml of chloroform which was already stirred on a magnetic stirrer (RT 15 power IKAMAG) and left for stirring for an hour to obtain well mixed solution. The resulting solution was spin coated on an aluminum foil at a speed of 1000rpm for 30 seconds. The coated aluminum foil was dried at 60°C for 12 hours to get the cathode film. Circular discs of diameter 15mm and mass ~0.5mg were cut from the film and used as cathodes in cells for performing the electrochemical characterizations. The thickness

achieved for this cathode was 23µm. Finally a coin cell was prepared (as mentioned in the section 'Preparation of Conventional Lithium Ion Coin Cells') by stacking the PVBPT based cathode and the rest of the components as mentioned in the above list.

2.2.5 Electrochemical measurements performed

The charge–discharge and cycling properties of the cell were evaluated between 0 and 4 V at different current densities using a PGSTAT (Metrohm Autolab) at room temperature. Cyclic Voltammetry (CV) measurement of the cell was conducted at a scan rate of 1mV/s between 0 and 4.

Electrochemical Impedance Spectroscopy (EIS) was done using the Metrohm Autolab at room temperature. The EIS measurements were performed with 10 mV perturbation amplitude in the range from 100 kHz to 10 mHz in automatic sweep mode from high to low frequencies. Data acquisition and analysis were done using Nova 1.6 software.

2.2.6 Preparation of flexible battery

Flexible bateries were prepared by sandwiching PEO between $LiCoO_2$ and graphite. They were rolled together to have good adhesion. They both have the dimensions of 22x22x0.0204mm. Figure 2-10(a) and (b) have 10% and 15% filled PEO as electrolyte respectively. Figure 2-10(c) explains the flexible nature of the prepared battery.

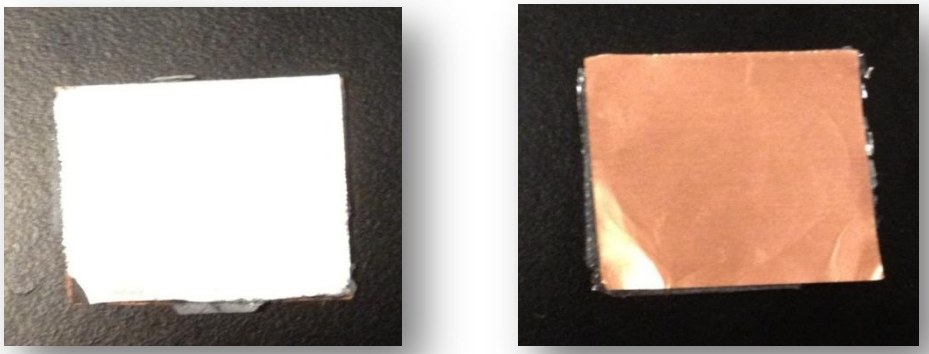

(a) (b)

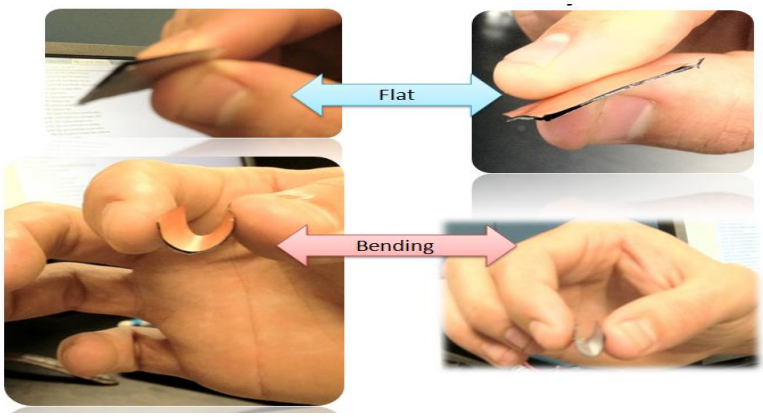

(c)

Figure 2-10. Flexible batteries (acknowledging Mejdi Kammoun and Eric Wood).

2.3 Preparation of Polymer samples for SEM imaging

A drop from pure or composite polymer solution is deposited onto a carbon black pasted on to a stub with a flat circular surface using a pipette. These stubs are heated in a vacuum oven at around 60°C or 70°C over 12 hours. The polymer, in itself, is electrically almost not conductive and hence not possible for micro structural studies using SEM. The organic polymer must allow a very small electrical conductivity to

transfer its electron to the carbon filler or viceversa. Hence it is coated with platinum using a sputter coater. Platinum is highly electrically conductive and enables the surface to be studied using SEM.

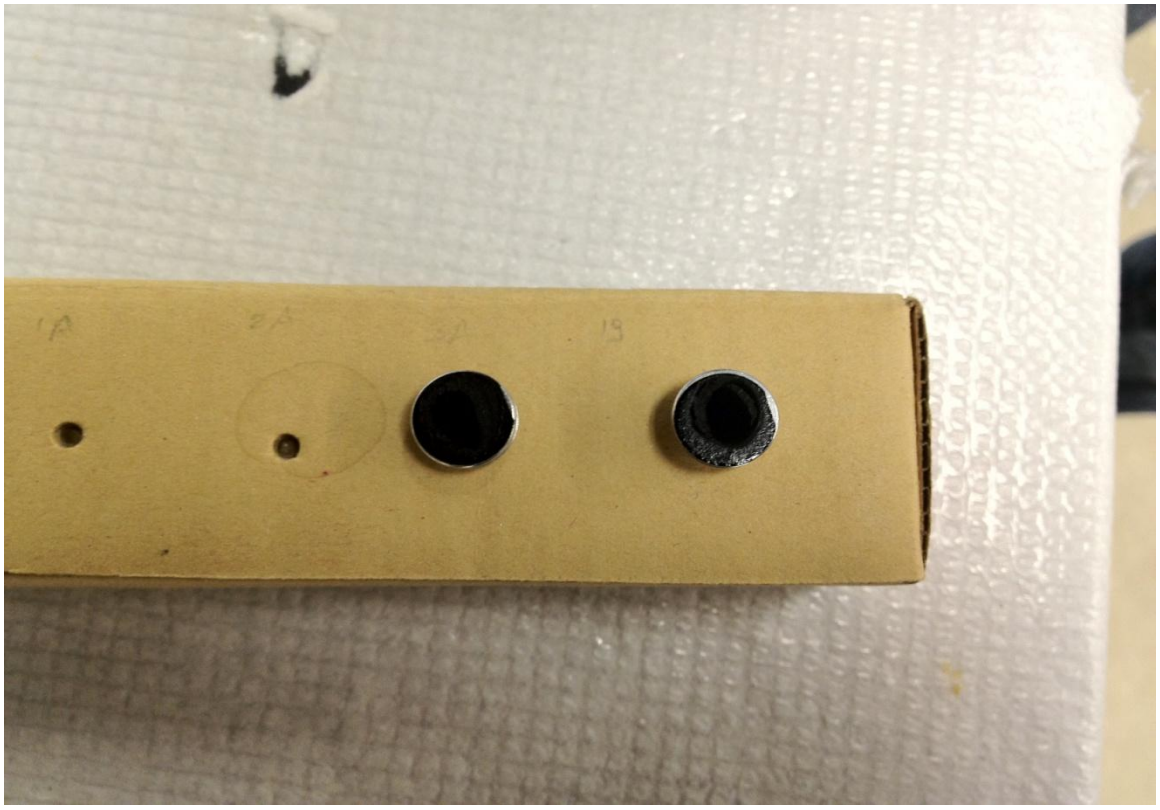

Figure 2-11. Composite polymer samples.

Figure 2-11 shows the composite polymer samples dried on a carbon tape which is pasted onto an SEM mount. These are sputter coated with either gold or platinum particles before being used in a Scanning Electron Microscope.

Chapter III: RESULTS and DISCUSSIONS

3.1 Cyclic Voltammetry

3.1.1 Conventional Lithium Ion coin cell (B1)

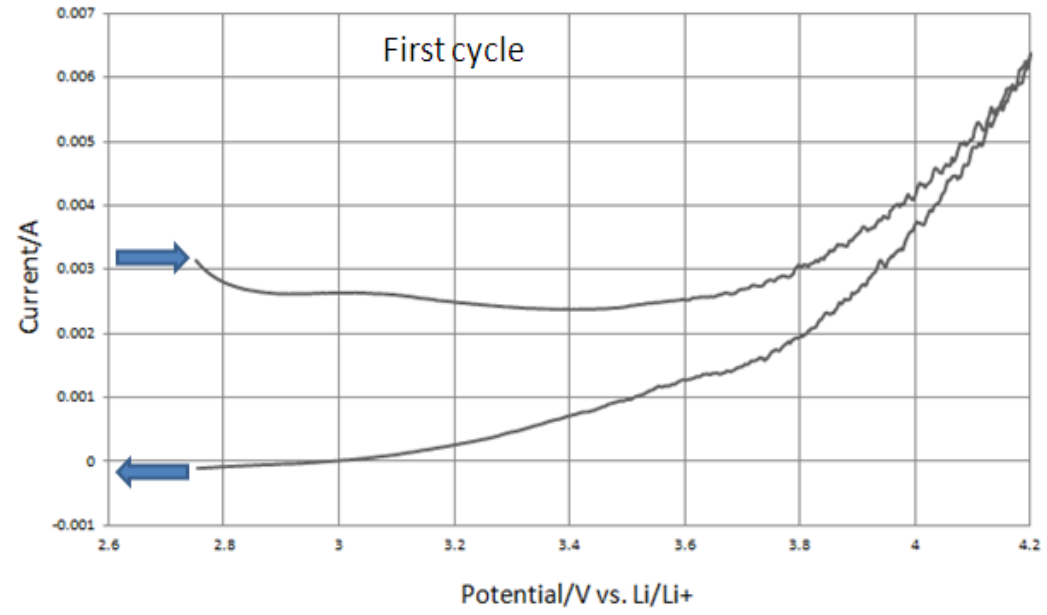

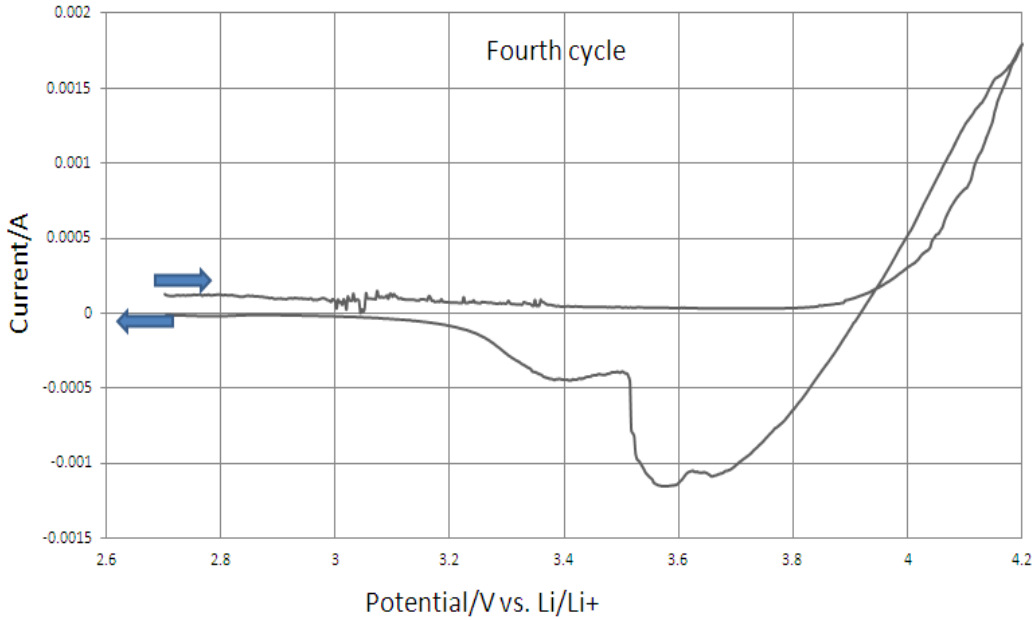

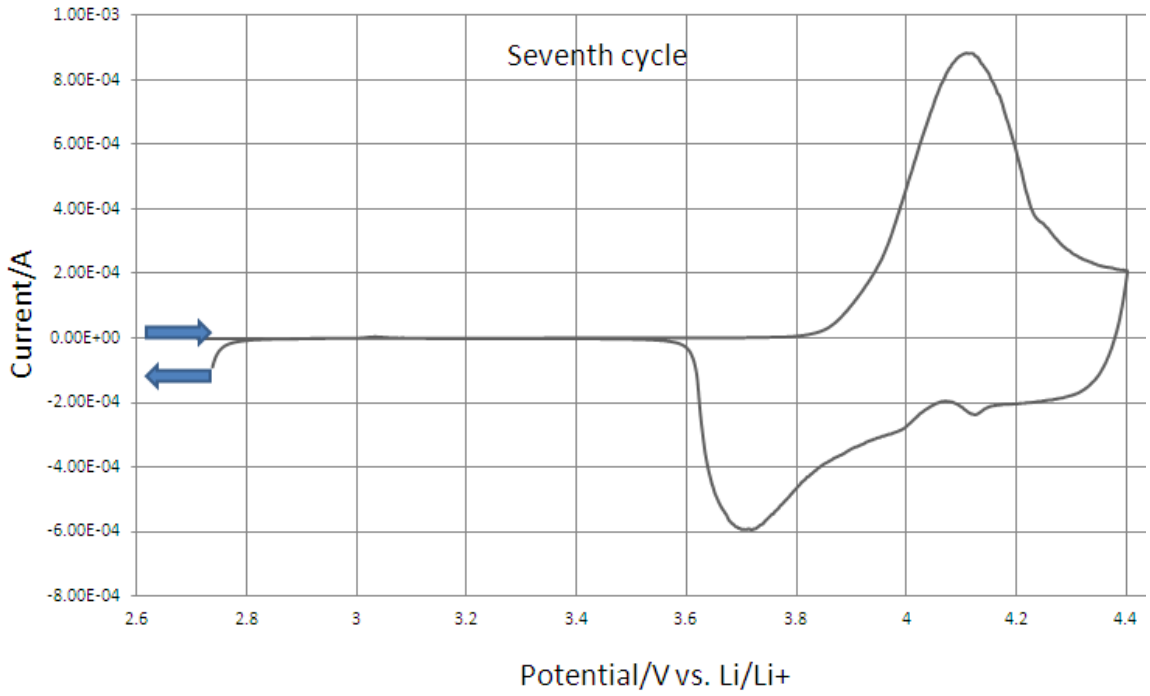

Figure 3-1. Cyclic voltammograms of $LiCoO_2$ cathode in 1 mol/L $LiPF_6$ in EC+DMC+DEC; 1:1:1 in volume, at various scan rates of 10mV/s, 100 µV/s and 10µV/s for the potential window of 2.7V to 4.4V.

From the three CV graphs, it can be inferred that $LiCoO_2$ cathode gives different current values at the same applied voltage at different scan rates. The first CV has no distinct oxidation (charging) and reduction (discharging) peaks and also only charging takes place all over the applied potential range. The second CV, though, exhibits charge and discharge activity over the entire potential range with distinct peaks it does not exhibit smooth flow and hence gives an illusion that battery might not be working properly at every applied voltage. The third CV exhibits charge and discharge activity within a certain potential window with distinct peaks. Now it can be said that the battery is fully functional. From the above three CVs it can be inferred that each battery

exhibits its own characteristic scan rate and that the fully functional nature of the battery is revealed only at that rate. This necessitates performing a CV test on the battery at different scan rates to capture the full functionality of it.

The following inferences can be made from the third CV:

Even though the applied potential window for the battery is 2.7V and 4.4V the redox activity occurs in the range of 3.6V and 4.4V. The onset of oxidation or charging start around 3.85V, reaches its peak at 4.1V and reaches the base line at around 4.38V. The discharge peaks occurs at 3.7V and reaches the base line at 3.6V. Hence the working potential for this cell at 10μV/s is 3.6 – 4.4V. The standard redox potential for this cell is 3.9 V vs. Li/Li^+. The maximum charging current is 0.87mA and occurs at 4.1V, the maximum discharging current is 0.6mA and occurs at 3.7V. The structural deformities occur in the $LiCoO_2$ cathode after 4.5V, hence the potential has not been ramped up beyond 4.4V to see whether the charging current reaches zero or not.

3.1.2 Pure PTMA based coin cell (B2)

Figure 3-2(a) refers to the first CV performed on the cell having pure PTMA cathode. It can be observed that only charging occurs over the entire potential window applied without any discharging. Along with the previous inference, the irregular data points on the curve give an illusion that the battery may not be functional.

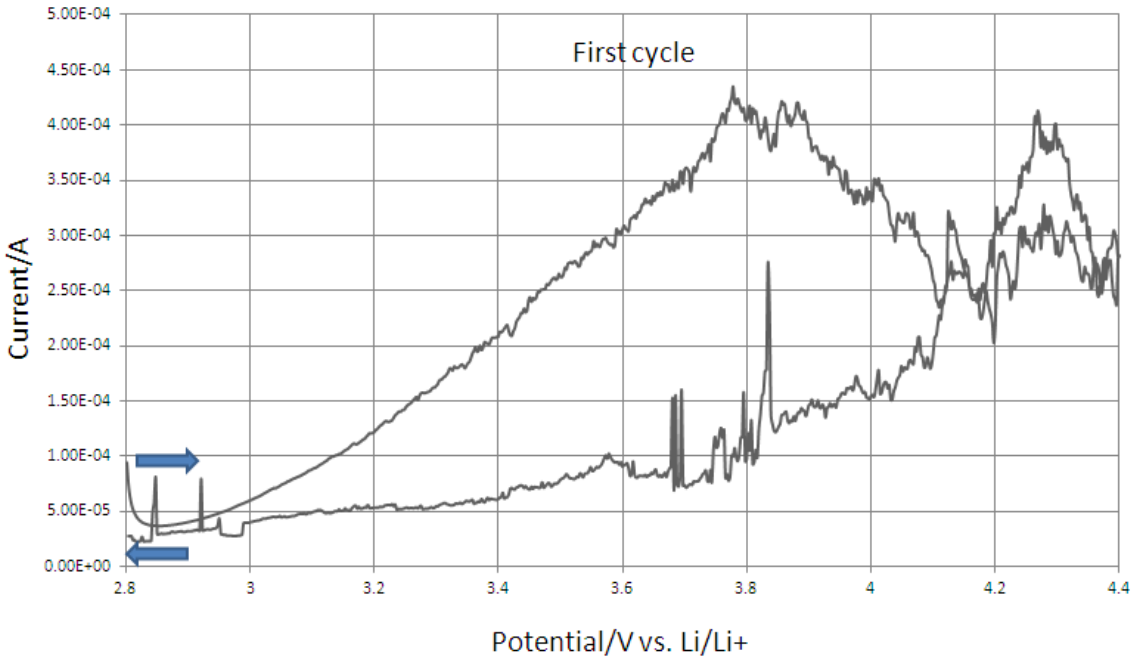

Figure 3-2(a). Cyclic voltammogram of pure PTMA cathode in 1 mol/L $LiPF_6$ in EC+DMC+DEC; 1:1:1 in volume, at various scan rates of 1mV/s for the potential window of 2.8V to 4.4V.

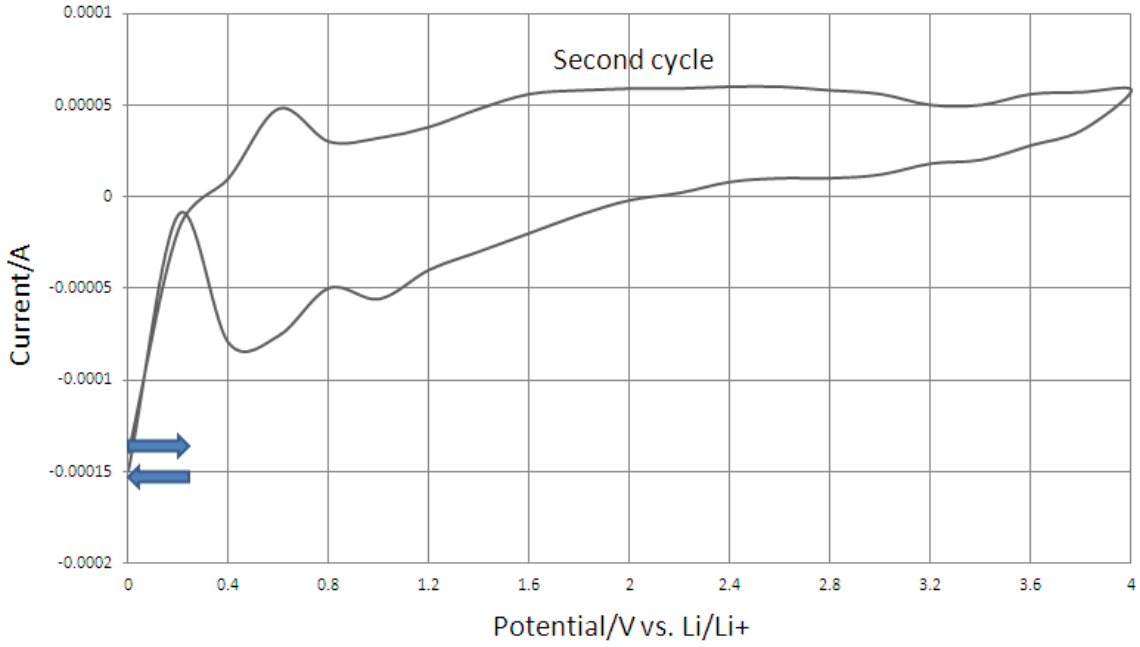

Figure 3-2(b). Cyclic Voltammogram of pure PTMA cathode in 1 mol/L $LiPF_6$ in EC+DMC+DEC; 1:1:1 in volume, at a scan rate of 10mV/s for the potential window of 0V to 4V.

Figure 3-2 refers to the second CV cycle performed on the cell. It can be observed that charging and discharging occurs throughout the applied potential window; and the cycle starts with discharging process because the cell has been only in the charging mode over the entire first cycle. Two charging peaks are occurred during the oxidation process. A narrow peak occurs at 0.6V with a maximum current value of 0.05mA and a broader one occurs at 2.4V with a current value of 0.06mA. A regular discharging peak has not been observed. A maximum discharging current of 0.14mA is occurred just before the applied potential reaches zero. From Figure 3-2(a) and Figure 3-2(b), 10mV/s can be termed as a characteristic scan rate PTMA based cathodes.

3.1.3 Composite PTMA based coin cell (B3)

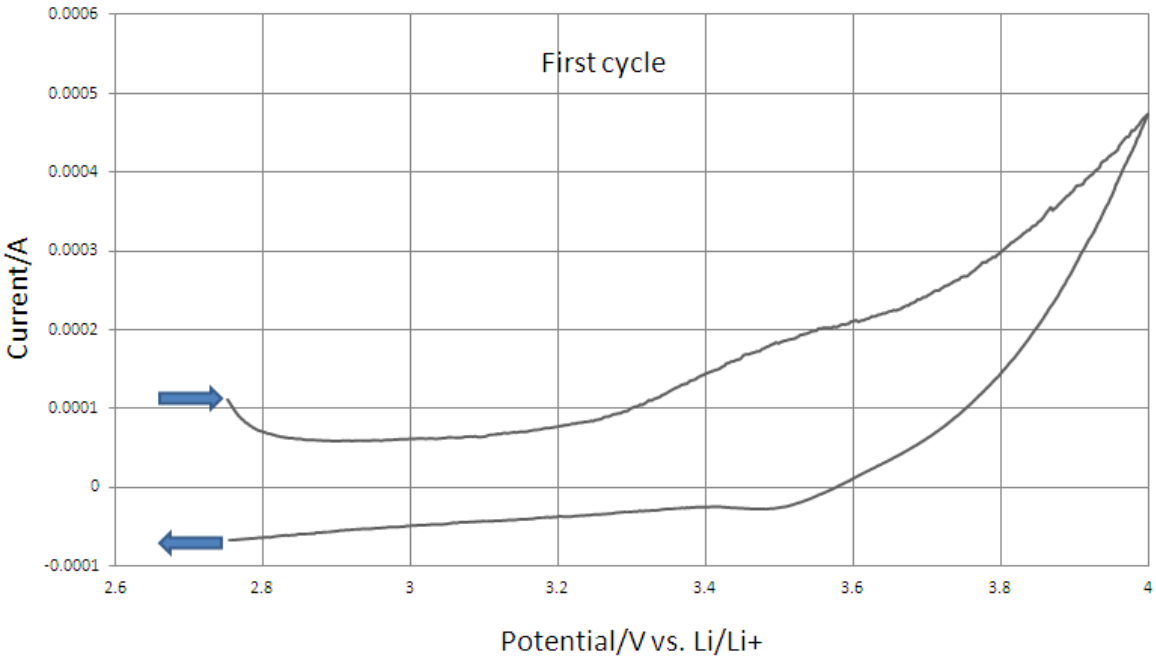

Figure 3-3(a). Cyclic Voltammogram of composite PTMA (polymer-10%, filler-70% and binder-20%) cathode in 1 mol/L $LiPF_6$ in EC+DMC+DEC; 1:1:1 in volume, at a scan rate of 10mV/s for the potential window of 2.75V to 4V.

The first CV sample test has been run on the cell between 2.75V and 4.0V. It can be observed from figure 3-3(a) that the battery is in charging mode for most of the applied potential and starts discharging only after reverse ramping of the potential at 3.58V. The cell is not completely discharged even after reaching the potential limit.

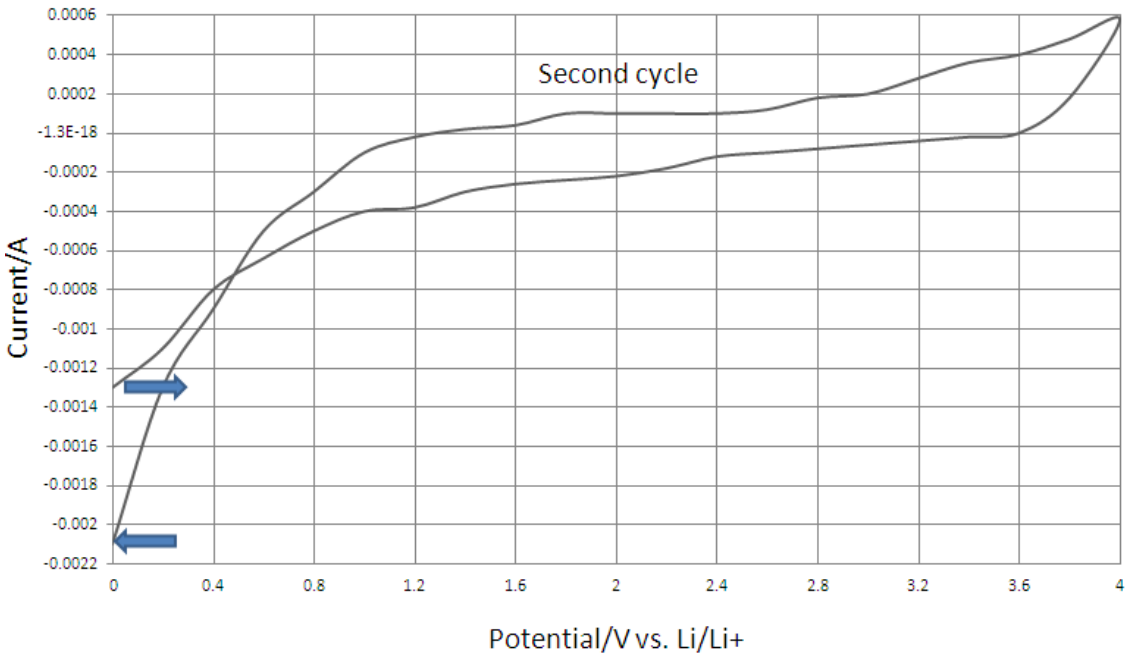

Figure 3-3(b). Cyclic Voltammogram of composite PTMA (polymer-10%, filler-70% and binder-20%) cathode in 1 mol/L $LiPF_6$ in EC+DMC+DEC; 1:1:1 in volume, at a scan rate of 10mV/s for the potential window of 0V to 4V.

Figure 3-3(b) indicates that the cell starts with discharging as the cell was not completely discharged during the previous cycle. The cell gets completely discharged at 1.3V and starts charging again. The maximum charging current is 0.6mA occurring and maximum discharging current is 2.1mA. From figure 3-3(a) and 3-3(b), it can be observed that the charging current has improved ten times whereas discharging current has improved hundred times. The increase in current can be attributed to the addition of filler (carbon particles). The charge and discharge peaks have not been observed.

3.1.4 Pure PVBPT based coin cell (B4)

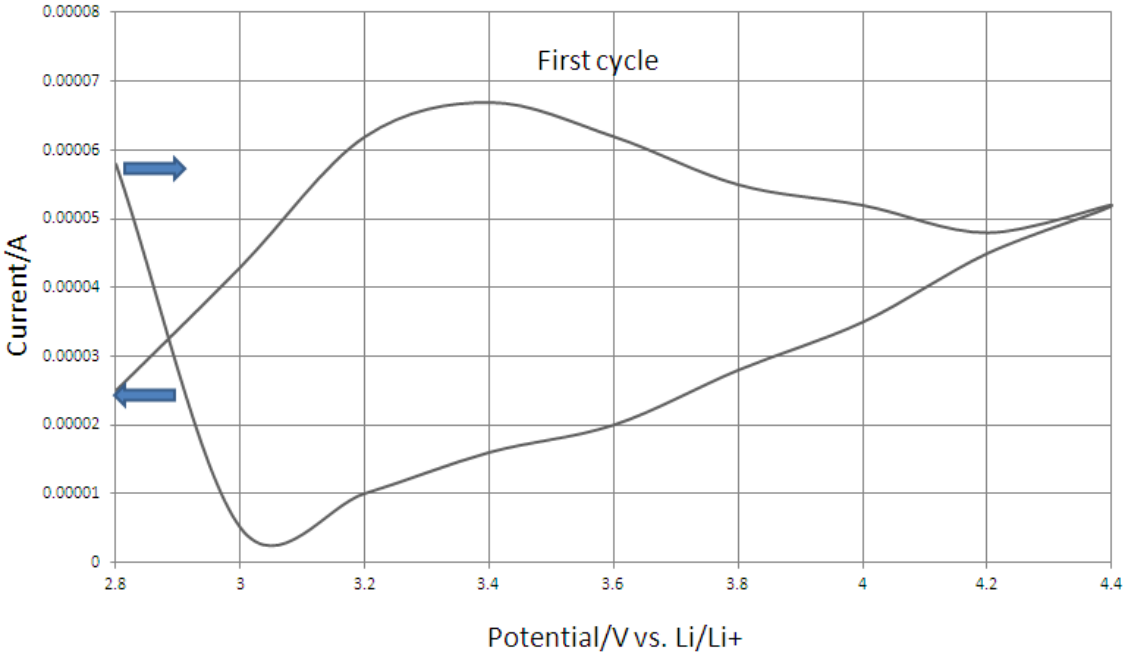

Figure 3-4(a). Cyclic Voltammogram of pure PVBPT cathode in 1 mol/L $LiPF_6$ in EC+DMC+DEC; 1:1:1 in volume, at a scan rate of 1mV/s for the potential window of 2.8V to 4V.

The first CV sample test has been run on the cell between 2.8V and 4.0V. It can be observed that the battery is in charging mode for the entire range of the applied potential.

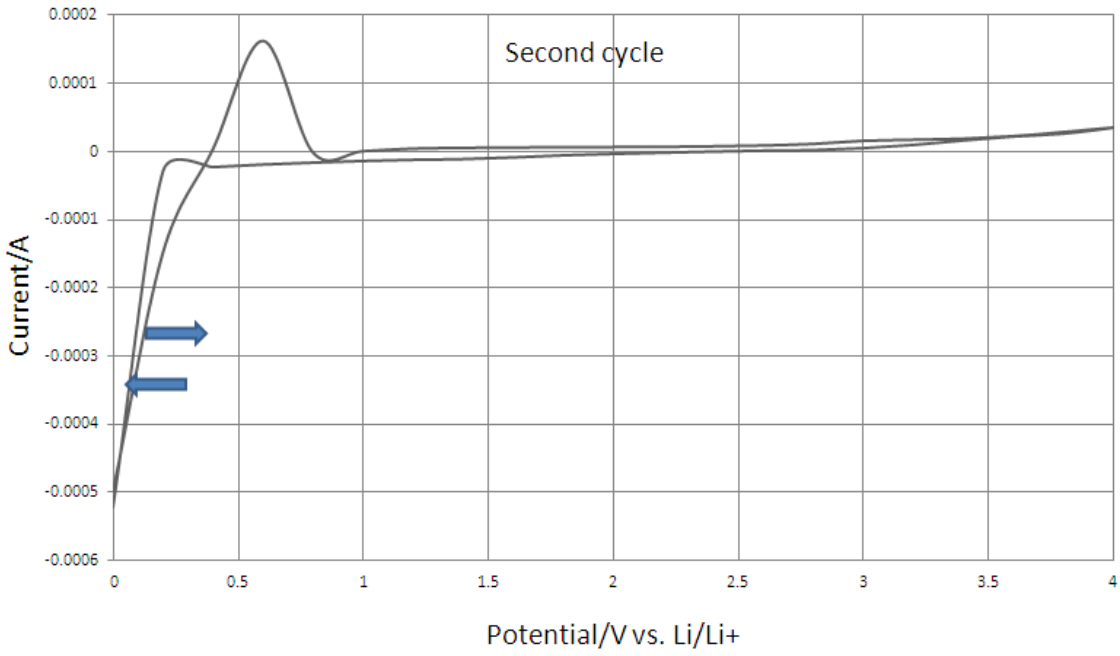

Figure 3-4(b). Cyclic Voltammogram of pure PVBPT cathode in 1 mol/L $LiPF_6$ in EC+DMC+DEC; 1:1:1 in volume, at a scan rate of 10mV/s for the potential window of 0V to 4V.

The above graph indicates that the cell starts with discharging as the cell was not completely discharged during the previous cycle. The cell is completely discharged at 0.4V and starts charging again. It shows a maximum charging peak at 0.6V with a charging a current of 0.18mA. The charging reaches zero at 0.8V and remains almost at the zero level even when the higher potential was applied and goes slightly above zero after 3V.The discharging starts at 2V and most of it occurs in the potential window of 0.2V to 0V. The discharge peak has not been occurred.

3.1.5 Polymer electrolyte based coin cell (B5)

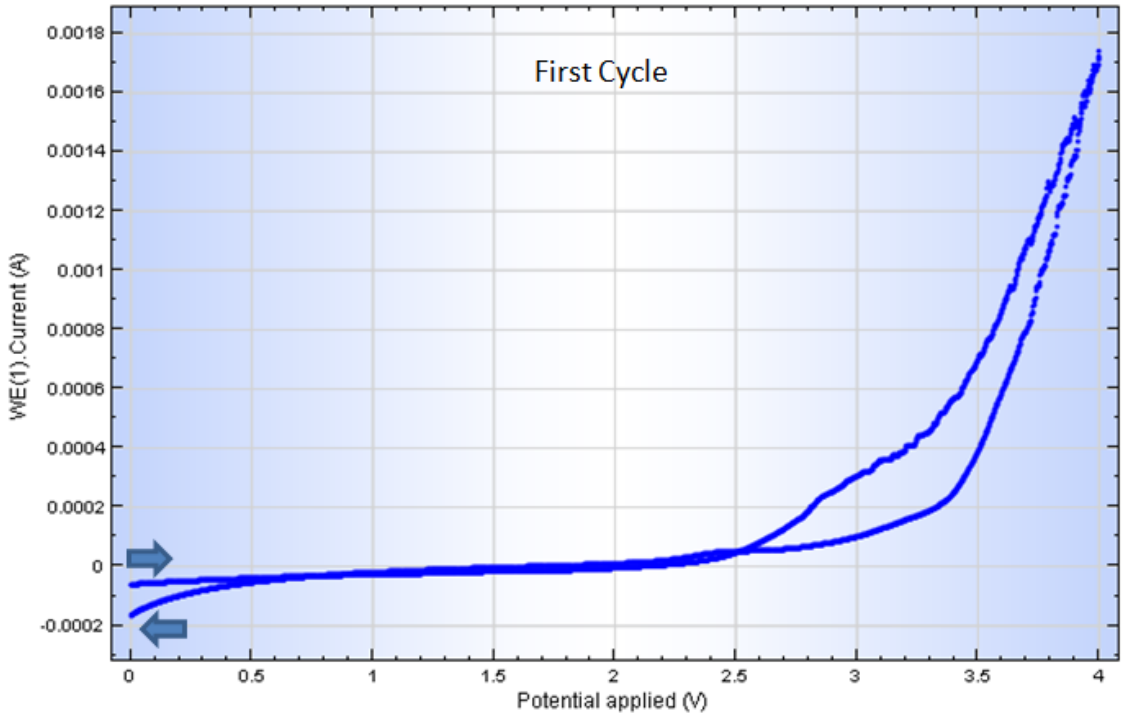

Potential / V vs. Li/Li^+

Figure 3-5. Cyclic voltammogram of a coin cell having pure PEO as electrolyte.

The above CV corresponds to a coin cell having $LiCoO_2$ cathode and graphite anode. It can be observed from the above picture that the CV has been applied from 0V to 4V. The battery starts charging from 2.4V and reaches a maximum of 0.17mA at 4V and starts decreasing as the potential is ramped backwards. The charging again reaches zero at 2.3V indicating the battery is completely charged and exhibits no changes till 0.5V, after which it starts discharging until the potential reaches 0V.

3.1.6 Flexible battery (B6 & B7)

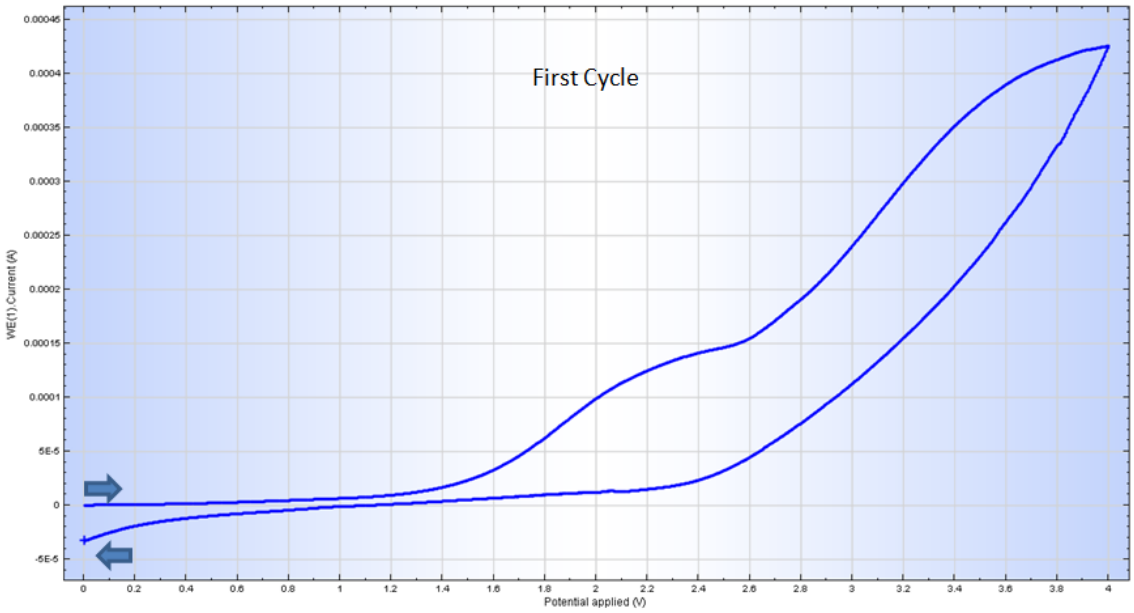

Potential / V vs. Li/Li^+

Figure 3-6. Cyclic voltammogram of a flexible battery having 10% filled PEO as electrolyte.

The above CV corresponds to a flexible battery having $LiCoO_2$ cathode and graphite anode. It can be observed from the above picture that the CV has been applied from 0V to 4V. The battery starts charging from 1.3V and reaches a maximum of 0.44mA at 4V and starts decreasing as the potential is ramped backwards. The charging again reaches zero at 1.3V indicating the battery is completely charged and exhibits no changes till 0.8V, after which it starts discharging until the potential reaches 0V.

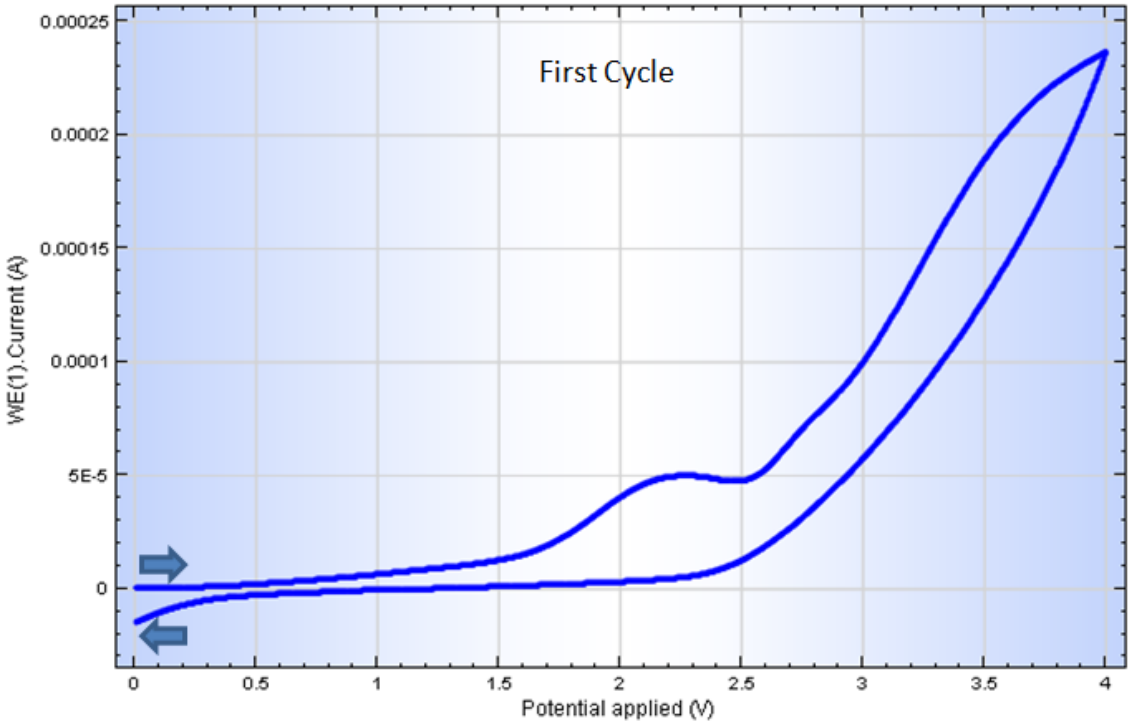

Figure 3-7. Cyclic voltammogram of a flexible battery having 15% filled PEO as electrolyte.

The above CV corresponds to a flexible battery having $LiCoO_2$ cathode and graphite anode. It can be observed from the above picture that the CV has been applied from 0V to 4V. The battery starts charging from 0.6V and reaches a maximum of 0.24mA at 4V and starts decreasing as the potential is ramped backwards. The charging again reaches zero at around 1.6V indicating the battery is completely charged and exhibits no changes till 0.4V, after which it starts discharging until the potential reaches 0V.

3.2 Energy and Efficiency:

3.2.1 Conventional Lithium Ion coin cell

Conventional Lithium Ion coin cell has exhibited charge and discharge capacities of 4.3mAh and 2.6mAh respectively. The calculated coulombic efficiency based on capacity for this particular cycle was 60%. The charge and discharge energies calculated from the above mentioned capacities were 54.644kJ and 33.134kJ respectively, exhibiting an energy efficiency of 61%.

3.2.2 Pure PTMA based coin cell

Pure PTMA based coin cell has exhibited charge and discharge capacities of 0.0054mAh and 0.0025mAh respectively. The calculated coulombic efficiency based on capacity for this particular cycle was 46%. The charge and discharge energies calculated from the above mentioned capacities were 44.5J and 10.7J respectively, exhibiting an energy efficiency of 24%.

3.2.3 Composite PTMA based coin cell

Composite PTMA based coin cell has exhibited charge and discharge capacities of 0.029mAh and 0.011mAh respectively. The calculated coulombic efficiency based on capacity for this particular cycle was 38%. The charge and discharge energies calculated from the above mentioned capacities were 302J and 80J respectively, exhibiting an energy efficiency of 26%.

3.2.4 Pure PVBPT based coin cell

Pure PVBPT based coin cell has exhibited charge and discharge capacities of 0.0097mAh and 0.0083mAh respectively. The calculated coulombic efficiency based on capacity for this particular cycle was 85%. The charge and discharge energies calculated from the above mentioned capacities were 67.2J and 51.7J respectively, exhibiting an energy efficiency of 77%.

3.3 Analysis of the Electrochemical Impedance Spectra

3.3.1 Conventional Lithium Ion coin cell

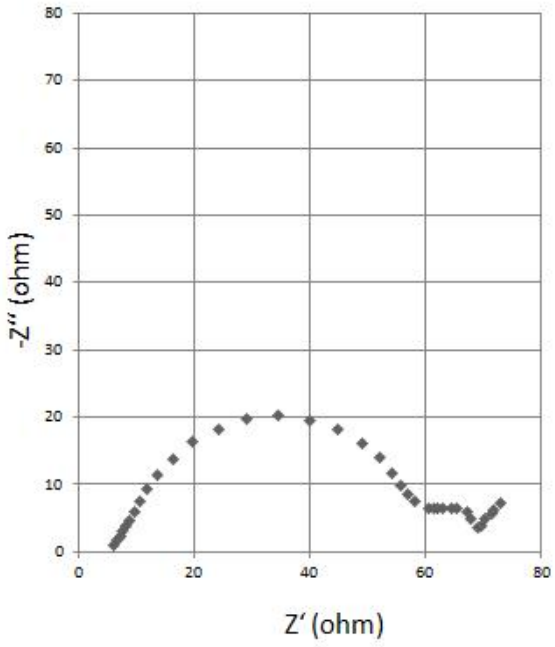

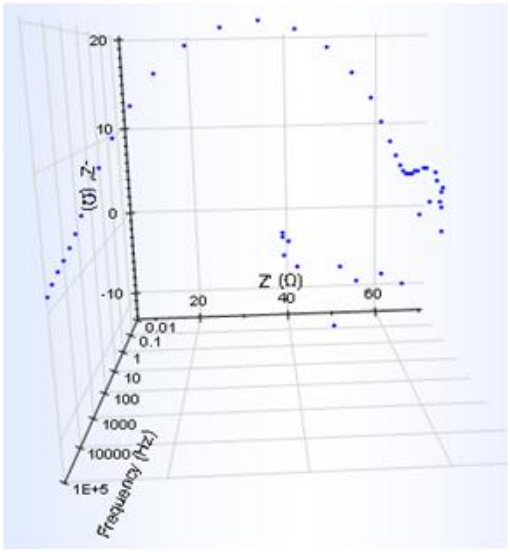

(a) **(b)**

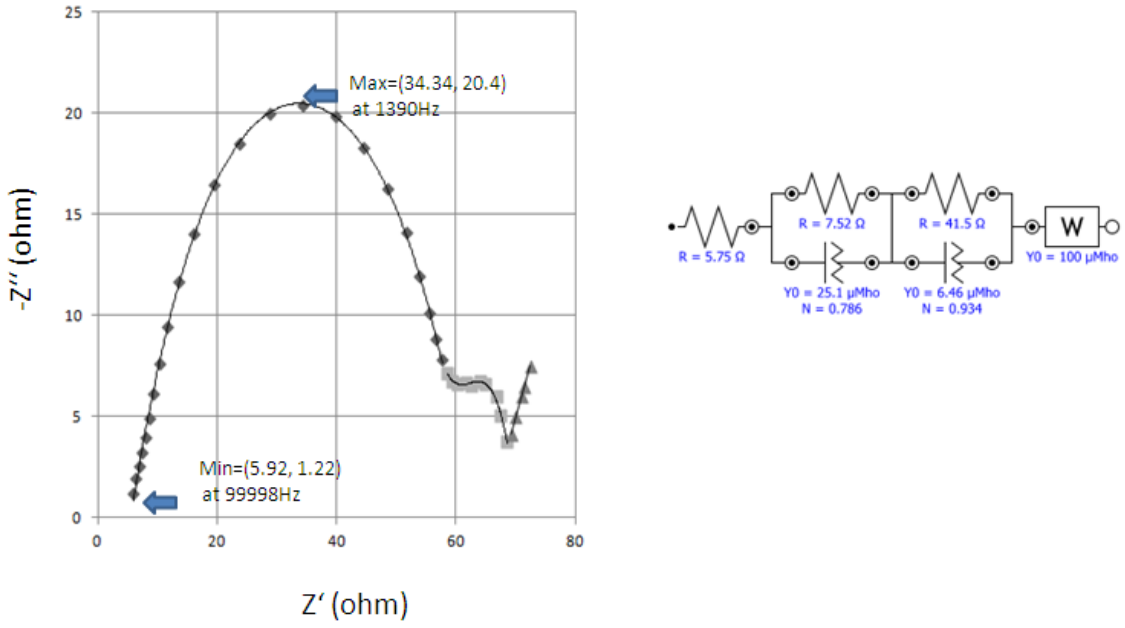

(c) **(d)**

Figure 3-8. EIS plot of $LiCoO_2$ cathode and its equivalent circuit fit.

Figure 3-8(a) displays the nyquist plot of the EIS obtained from the $LiCoO_2$ cathode at the total discharged state after seven cycles of charge and discharge process. For the $LiCoO_2$ cathode at the initial state after seven cycles, one dispersed semicircle spanning from high frequency region to low frequency region, another restricted semicircle and a restricted beeline at low frequency region was observed. Figure 3-8(b) displays the three dimensional view of the nyquist plot which shows impedance values sampled at applied frequency. Figure 3-8(c) represents the magnified version of plot (a) along with the fitted lines. Figure 3-8(d) displays the equivalent circuit used for fitting and simulating the obtained nyquist plot. The first resistance element, R=5.75Ω, corresponds to the contact and electrolyte resistance (Re); the second resistance

element, R=7.52Ω, corresponds to the charge transfer resistance (Rct); the third resistance element, R=41.5Ω, corresponds to the surface film resistance (Rsf). Two Constant Phase Elements (CPE) connected parallel to Rct, Rsf and have been introduced instead of a pure capacitive element to represent the double layer capacitance of the surface film. A CPE has been introduced to model the behavior of surface film as an imperfect capacitor as the obtained impedance spectra corresponds to a battery which already run several cycles. The approximate beeline is represented by Warburg impedance which corresponds to the diffusion of Lithium-ion in the cathode.

3.3.2 Pure PTMA based coin cell

Figure 3-9(a) displays the nyquist plot of the EIS obtained from the pure PTMA based cathode at the total discharged state after seven cycles of charge and discharge process. For the PTMA cathode at the initial state after seven cycles, one dispersed semicircle spanning from high frequency region to low frequency region was observed. The first semicircle corresponds to the surface film resistance. The EIS data beyond the first semicircle is inconclusive. There appears to be a curvature indicating a semicircle corresponding to charge transfer impedance and a line corresponding to warburg impedance, although not observed completely in this scan. Further verifications require performing the experiment at very low frequencies to validate the above inference regarding charge transfer and warburg impedance.

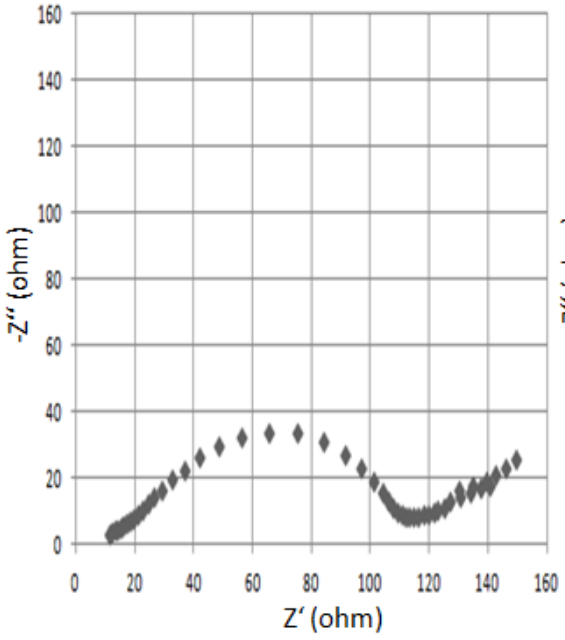
-Z'' (ohm)
Z' (ohm)

(a)

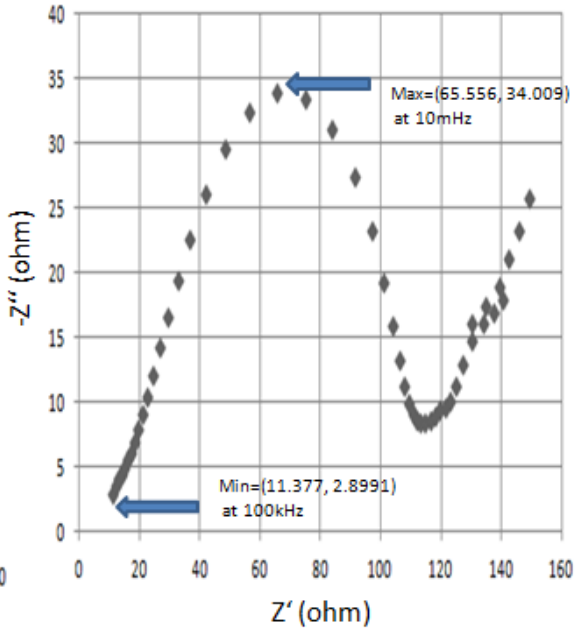
Max=(65.556, 34.009)
at 10mHz
Min=(11.377, 2.8991)
at 100kHz
-Z'' (ohm)
Z' (ohm)

(b)

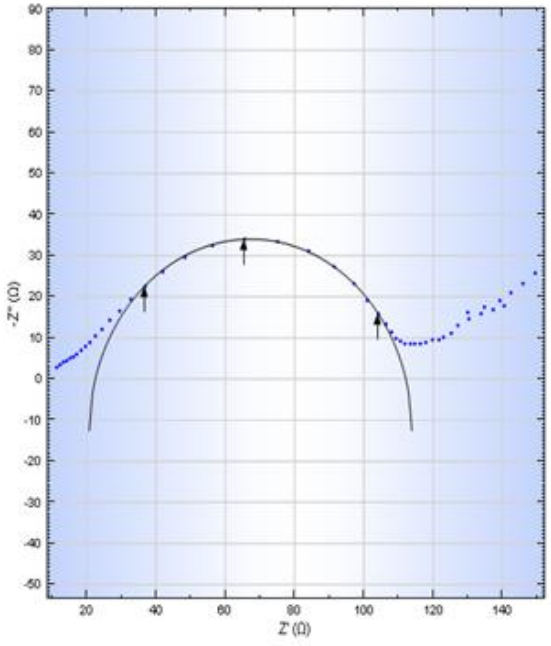
-Z'' (Ω)
Z' (Ω)

(c)

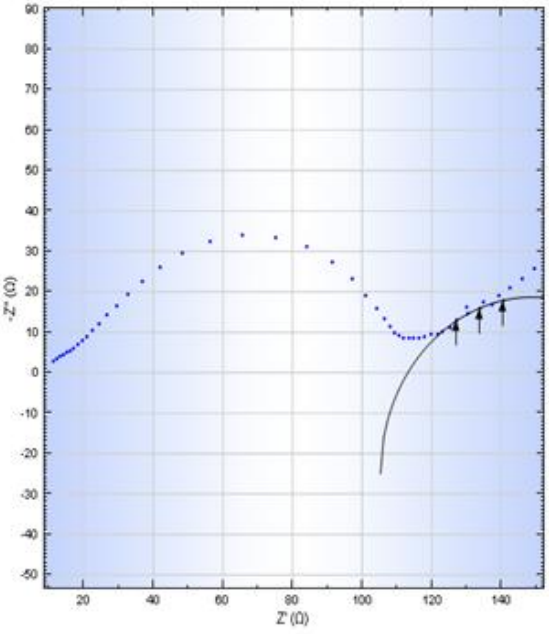
-Z'' (Ω)
Z' (Ω)

(d)

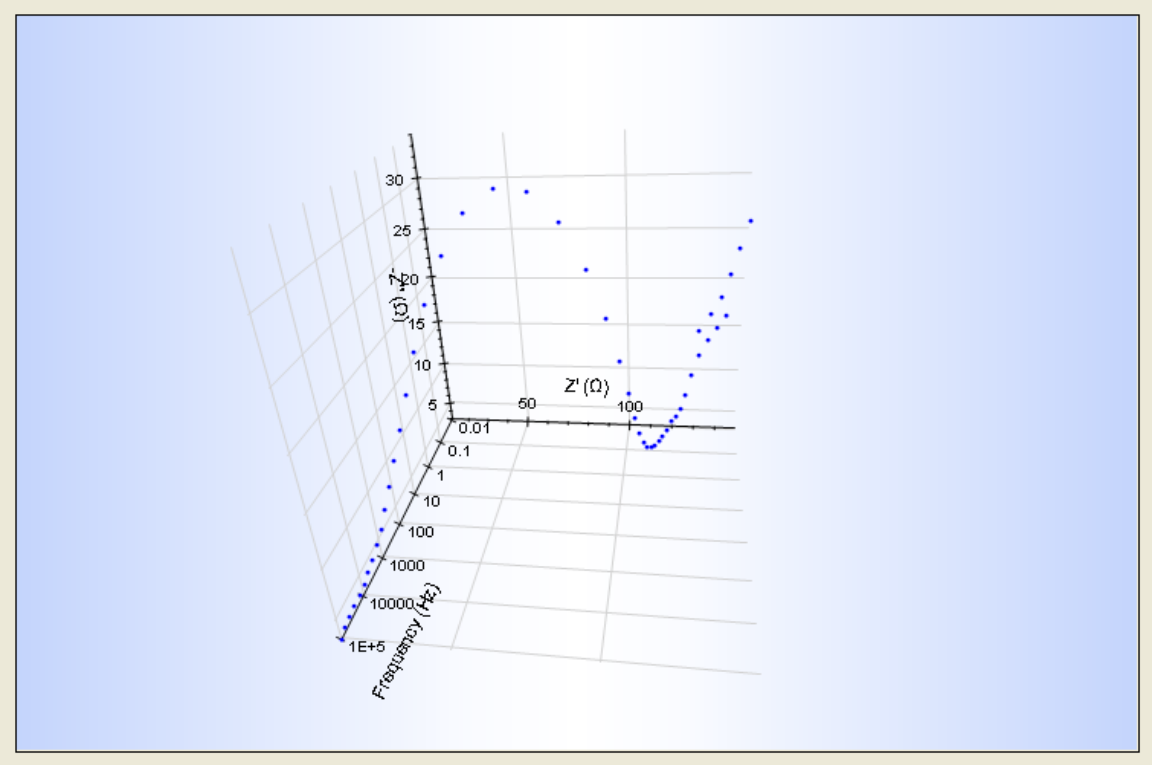

(e)

Figure 3-9. EIS plots of PTMA cathode.

Figure 3-9(c) and Figure 3-9(d) displays the equivalent electrochemical circle fitting for the obtained nyquist plot. The first resistance element (distance between the origin and the first plotted impedance value at high frequency), R=11.1Ω, corresponds to the contact and electrolyte resistance (Re); The diameter of the fitted semicircle in Figure 3-9(c) corresponds to the surface film resistance (Rsf) which was 90 Ω. In each electrochemical circle fitting the circle is assumed as a constant phase element (CPE) and a resistor connected in parallel. A CPE has been introduced instead of pure capacitive element to represent the double layer capacitance of the surface film. A CPE

has been introduced to model the behavior of surface film as an imperfect capacitor as the obtained impedance spectra corresponds to a battery which already run several cycles. The diameter of the fitted semicircle in Figure 3-9(d) corresponds to the charge transfer resistance (Rct) which was 53.24Ω. Figure 3-9(e) displays the three dimensional view of the nyquist plot which shows impedance values sampled at applied frequency.

3.3.3 Composite PTMA based coin cell

Figure 3-10(a) displays the nyquist plot of the EIS obtained from the composite PTMA based cathode at the total discharged state (2.8V) after ten cycles of charge and discharge process. For the composite PTMA cathode at the initial state after ten cycles, one dispersed semicircle, spanning from high frequency region to low frequency region was observed. The first semicircle corresponds to the surface film resistance. The EIS data beyond the first semicircle is inconclusive. There appears to be a curvature indicating a large semicircle corresponding to very large charge transfer impedance. warburg impedance is expected to follow, although not observed in this scan. Further verifications require performing the experiment at very low frequencies to validate the above inference regarding charge transfer and warburg impedance. The large transfer impedance may indicate very weak transfer of electrons and weak chemical reactions between Lithium and electrode material.

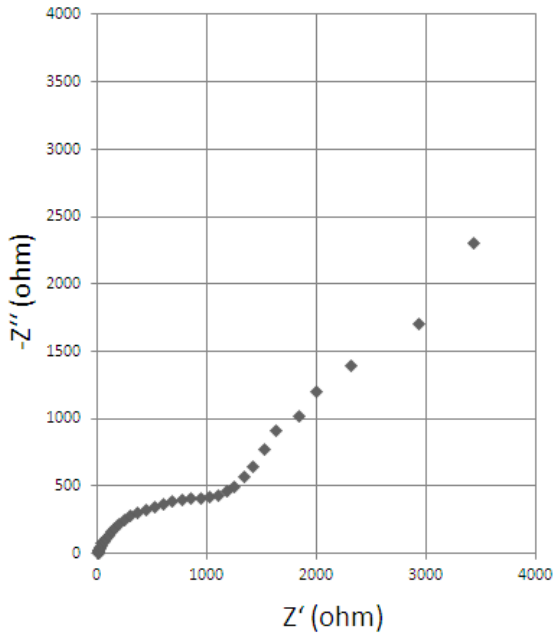
-Z'' (ohm)
Z' (ohm)
0
500
1000
1500
2000
2500
3000
3500
4000

(a)

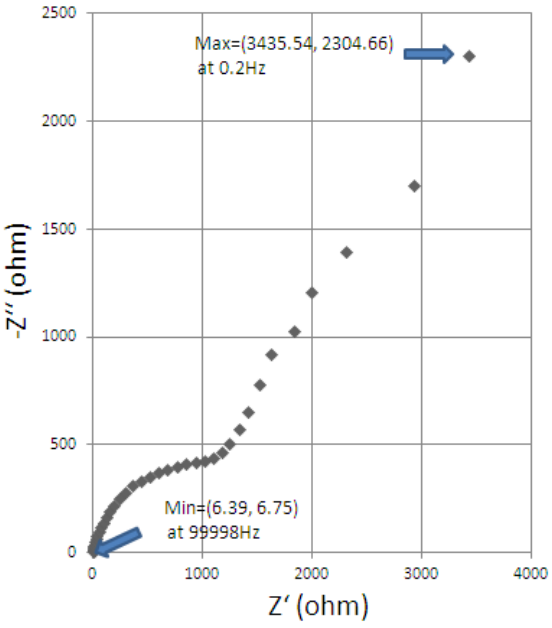
Max=(3435.54, 2304.66)
at 0.2Hz
Min=(6.39, 6.75)
at 99998Hz
-Z'' (ohm)
Z' (ohm)
0
500
1000
1500
2000
2500
3000
4000

(b)

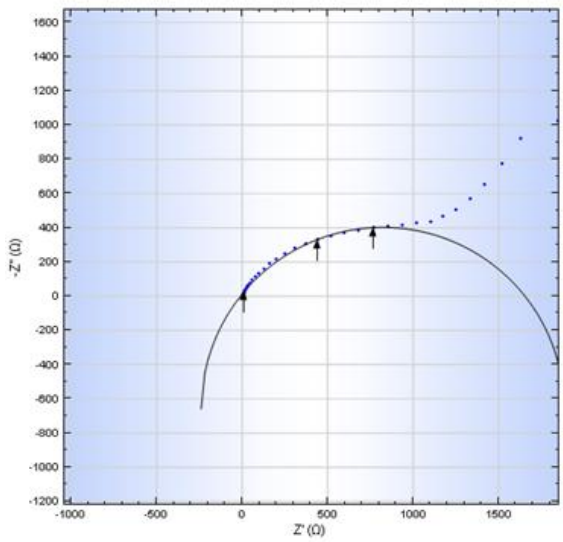
-Z'' (Ω)
Z' (Ω)

(c)

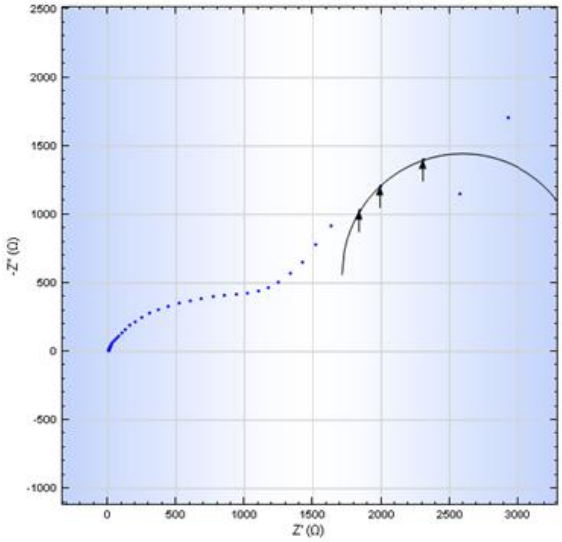
-Z'' (Ω)
Z' (Ω)

(d)

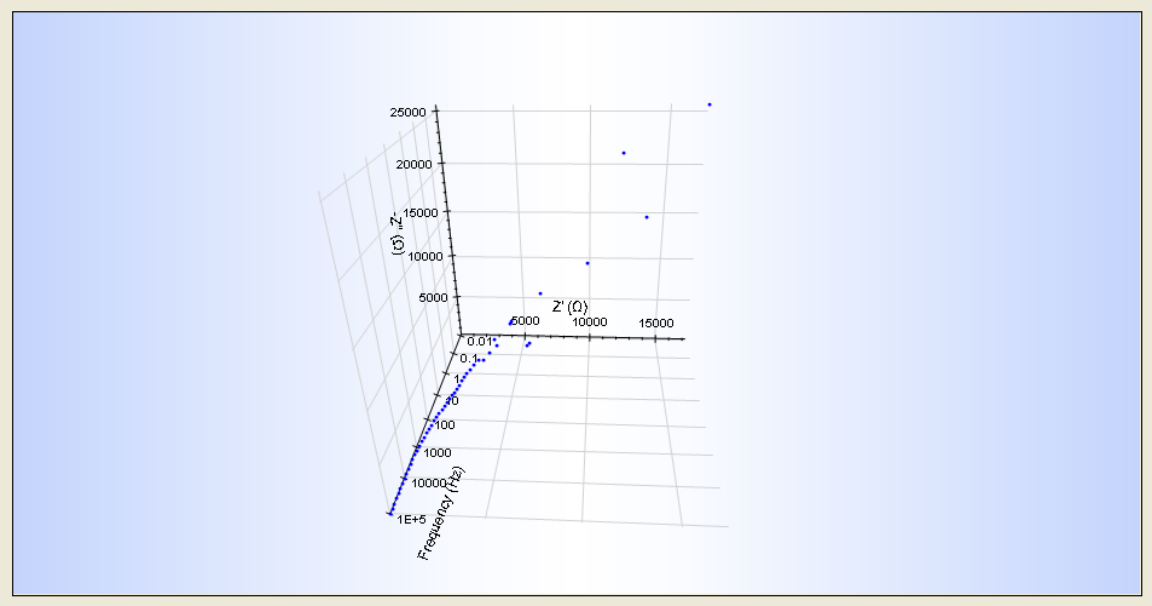

(e)

Figure 3-10. EIS plots of composite PTMA cathode.

Figure 3-10(c) and Figure 3-10(d) displays the equivalent electrochemical circle fitting for the obtained nyquist plot. The first resistance element (distance between the origin and the first plotted impedance value at high frequency), R=17.2Ω, corresponds to the contact and electrolyte resistance (Re). The diameter of the fitted semicircle in Figure 3-10(c) corresponds to the surface film resistance (Rsf) which was 1.5kΩ. In each electrochemical circle fitting the circle is assumed as a constant phase element (CPE) and a resistor connected in parallel. A CPE has been introduced instead of pure capacitive element to represent the double layer capacitance of the surface film. A CPE has been introduced to model the behavior of surface film as an imperfect capacitor as the obtained impedance spectra corresponds to a battery which already run several cycles. The diameter of the fitted semicircle in Figure 3-10(d) corresponds to the charge

transfer resistance (Rct) which was 5.6kΩ. Figure 3-10(e) displays the three dimensional view of the nyquist plot which shows impedance values sampled at applied frequency.

3.3.4 Pure PVBPT based coin cell

Figure 3-11(a) displays the nyquist plot of the EIS obtained from the pure PVBPT based cathode at the total discharged state after five cycles of charge and discharge process. For the PVBPT cathode at the initial state after five cycles, one dispersed semicircle, spanning from high frequency region to low frequency region was observed. The first semicircle corresponds to the surface film resistance. The EIS data beyond the first semicircle is inconclusive. There appears to be a curvature indicating a semicircle corresponding to charge transfer impedance and a line corresponding to warburg impedance, although not observed completely in this scan. Further verifications require performing the experiment at very low frequencies to validate the above inference regarding charge transfer and warburg impedance.

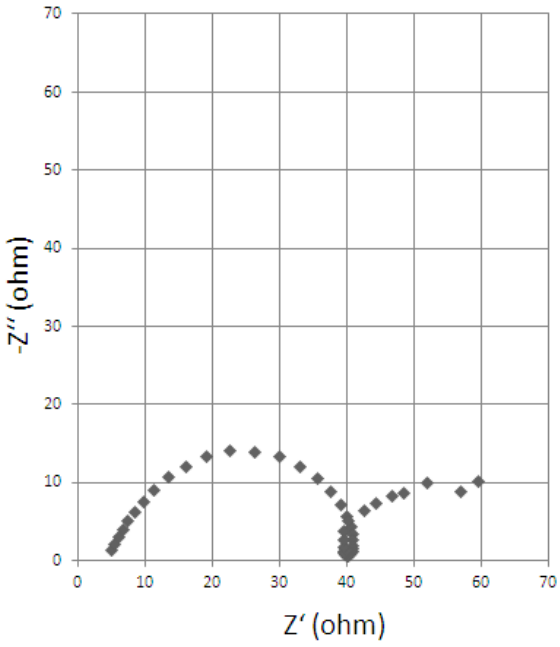
-Z'' (ohm)
Z' (ohm)

(a)

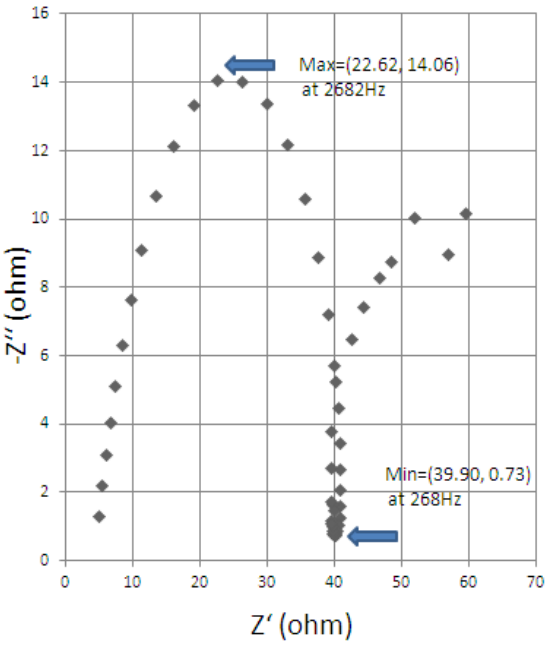
Max=(22.62, 14.06)
at 2682Hz
Min=(39.90, 0.73)
at 268Hz
-Z'' (ohm)
Z' (ohm)

(b)

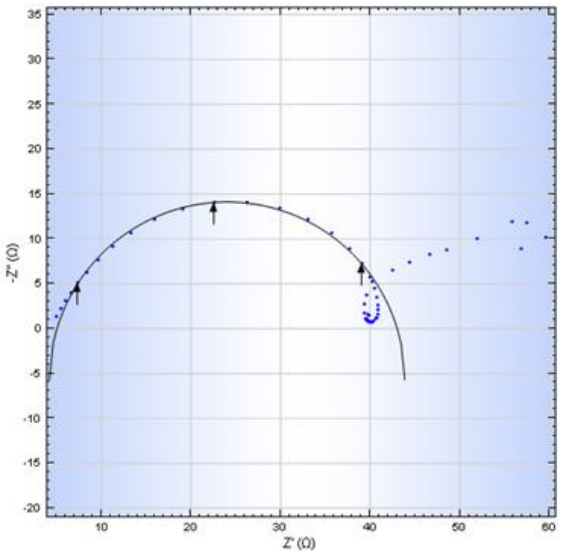
-Z'' (Ω)
Z' (Ω)

(c)

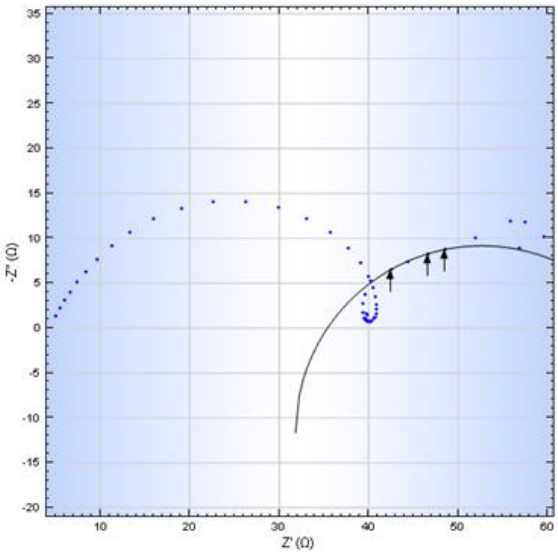
-Z'' (Ω)
Z' (Ω)

(d)

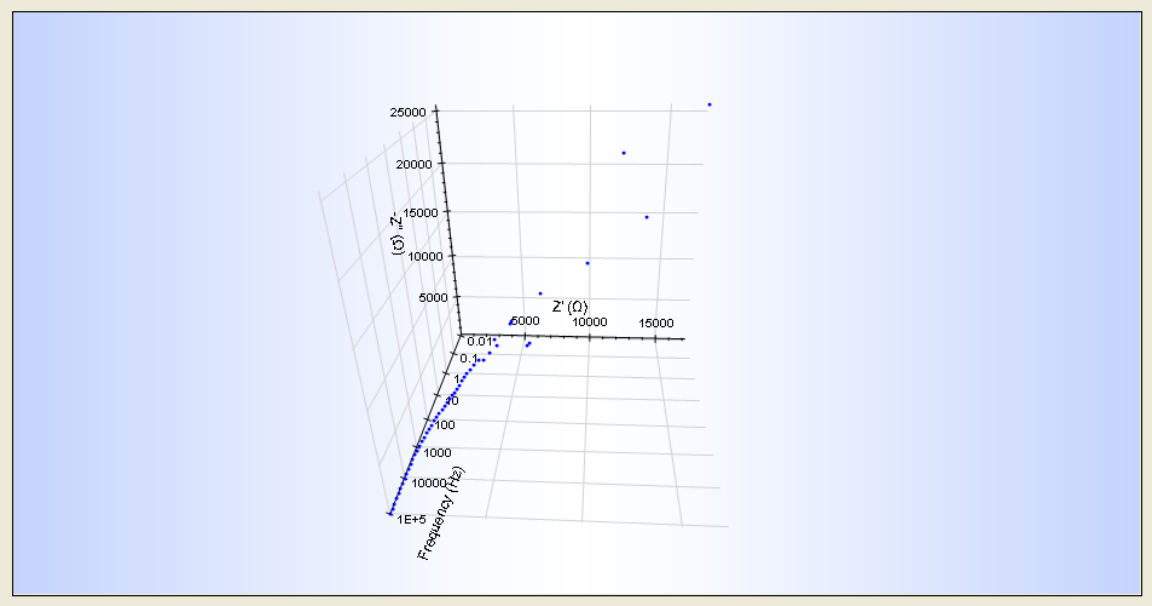

(e)

Figure 3-11. EIS plots of PVBPT cathode.

Figure 3-11(c) and Figure 3-11(d) displays the equivalent electrochemical circle fitting for the obtained nyquist plot. The first resistance element (distance between the origin and the first plotted impedance value at high frequency), R=4.73Ω, corresponds to the contact and electrolyte resistance (Re). The diameter of the fitted semicircle in Figure 3-11(c) corresponds to the surface film resistance (Rsf) which was 38.4Ω. In each electrochemical circle fitting the circle is assumed as a constant phase element (CPE) and a resistor connected in parallel. A CPE has been introduced instead of pure capacitive element to represent the double layer capacitance of the surface film. A CPE has been introduced to model the behavior of surface film as an imperfect capacitor as the obtained impedance spectra corresponds to a battery which already run several cycles. The diameter of the fitted semicircle in Figure 3-11(d) corresponds to the charge

transfer resistance (Rct) which was 24.7Ω. Figure 3-11(e) displays the three dimensional view of the nyquist plot which shows impedance values sampled at applied frequency.

3.4 Analysis of the Scanning Electron Microscope (SEM) Images

Figure 3-12(a) and Figure 3-12(b) represents the images of pure PTMA layer taken at a magnification of 10000X - 3µm and 59310X – 300nm respectively. From the above images it can be observed that the pure polymer exhibits flake like morphology along with irregular spherical like particles on its surface and exists in its glassy state at room temperature. The irregularities might be arising during the process of making the polymer solution and drying it on to a holder for SEM imaging purposes.

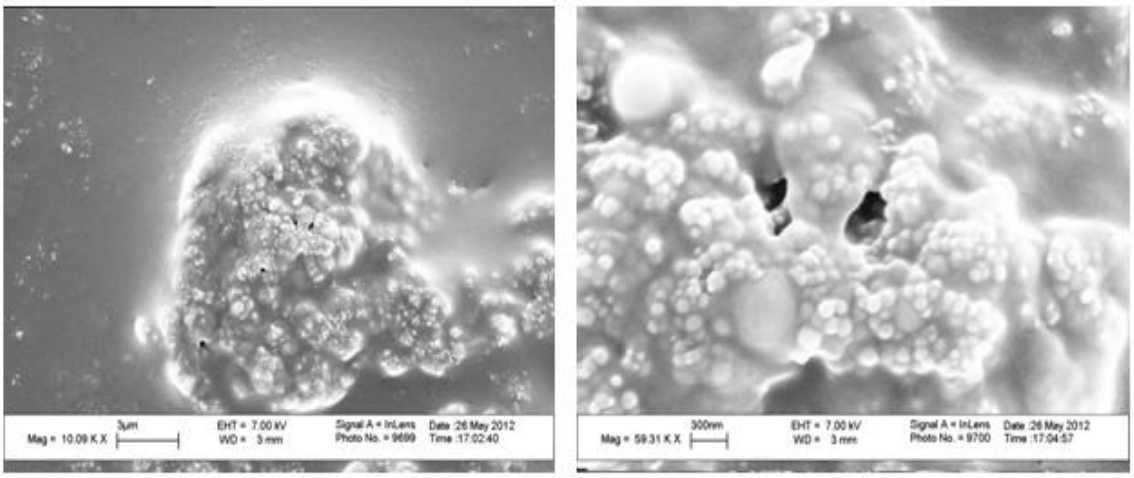

(a) **(b)**

Figure 3-12. SEM images of Pure PTMA sputter coated with gold particles.

Figure 3-13(a) and Figure 3-13(b) represents the images of pure PTMA layer taken at a magnification of 15000X - 1µm and 65000X – 200nm respectively. The same analysis given for the above section applies for the platinum coated images. It can also be observed that platinum coating yields better images compared to the gold coating.

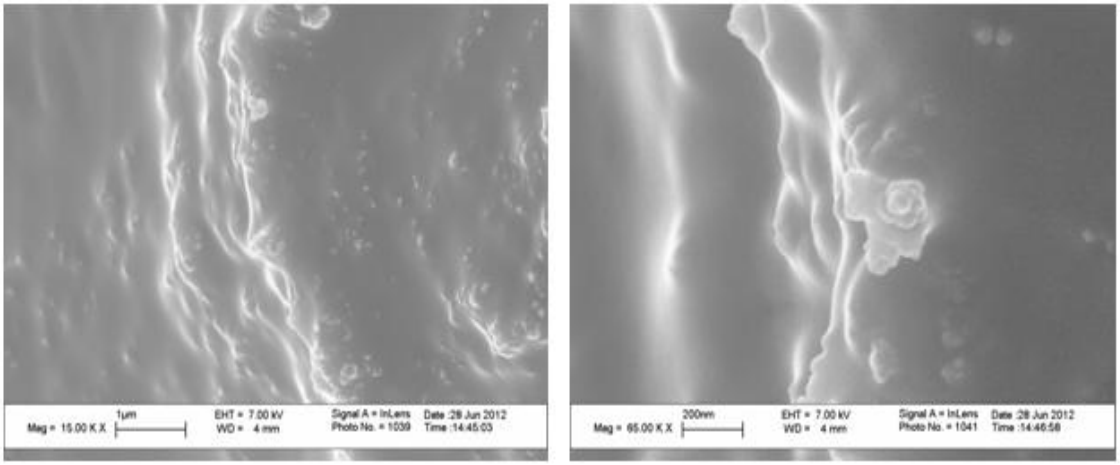

(a) **(b)**

Figure 3-13. SEM images of Pure PTMA sputter coated with platinum.

Figure 3-14(a) and Figure 3-14(b) represents the images of composite PTMA layer taken at a magnification of 10000X - 1µm and 44640X – 1µm respectively. The composite polymer shows carbon particles (filler), spherical in shape which were coated with a thin layer of polymer while making the composite solution for cathode preparation. It can be observed from the above SEM images that the polymer layer coating over the carbon particles is very thin and show well-defined particle morphology. If more polymer is used in composite solution rather than filler, the polymer layers will fuse together and give a flake-like morphology.

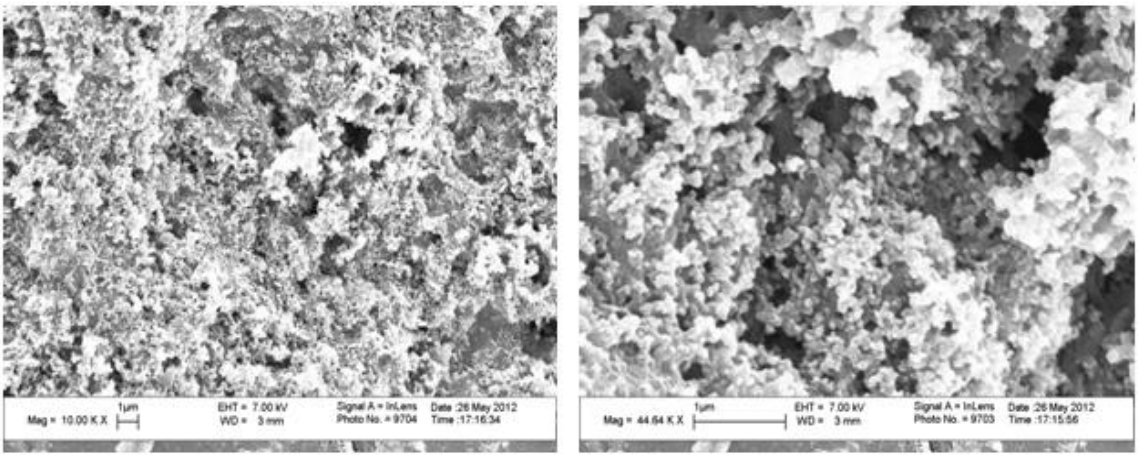

(a) **(b)**

Figure 3-14. SEM images of composite PTMA (PTMA – 10%, Filler – 70%, Binder – 20%) sputter coated with gold particles.

Comparison of figure 3-15 with figure 3-14 supports the fact that the polymer is electrically almost insulating and that requires coating for SEM studies and filler that supports electronic conductivity for electrochemical studies. Even though the filler is electronically conductive sputter coating the composite sample shows better surface morphology.

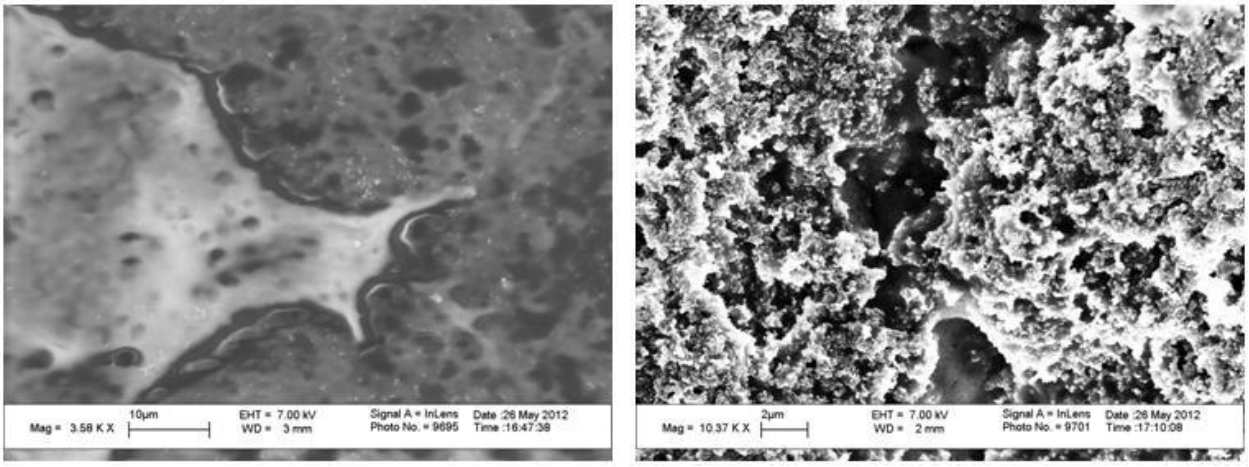

(a) **(b)**

Figure 3-15. SEM images of uncoated Pure PTMA and Composite PTMA.

Figure 3-16(a) and figure 3-16(b) represents the images of pure PVBPT layer taken at a magnification of 6500X - 2µm and 45000X – 200nm respectively. From the above images it can be observed that the pure polymer exhibits flake like morphology along with irregular spherical like particles on its surface and exists in its glassy state at room temperature. The irregularities might be arising during the process of making the polymer solution and drying it on to a holder for SEM imaging purposes.

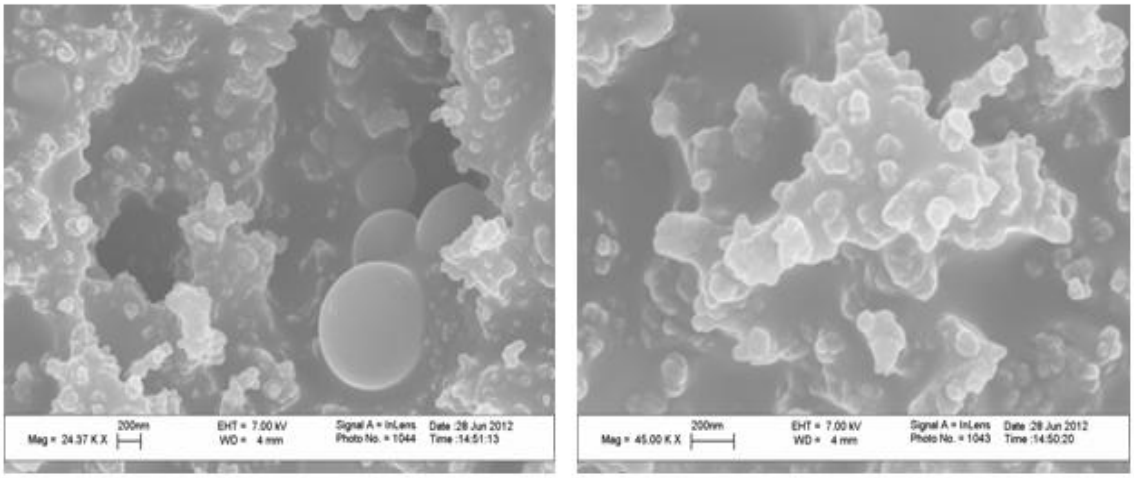

(a) **(b)**

Figure 3-16. SEM images of Pure PVBPT sputter coated with platinum.

Figure 3-17(a) and figure 3-17(b) represents the images of composite PVBPT layer taken at a magnification of 10000X - 2µm and 20000X – 1µm respectively. The composite polymer shows carbon particles (filler), spherical in shape which got coated with a thin layer of polymer while making the composite solution for cathode preparation. It can be observed from the above SEM images that the polymer layer coating over the carbon particles is very thin and that they show a well-defined particle morphology. If more polymer is used in composite solution rather than filler, the polymer layers will fuse together and gives a flake like morphology.

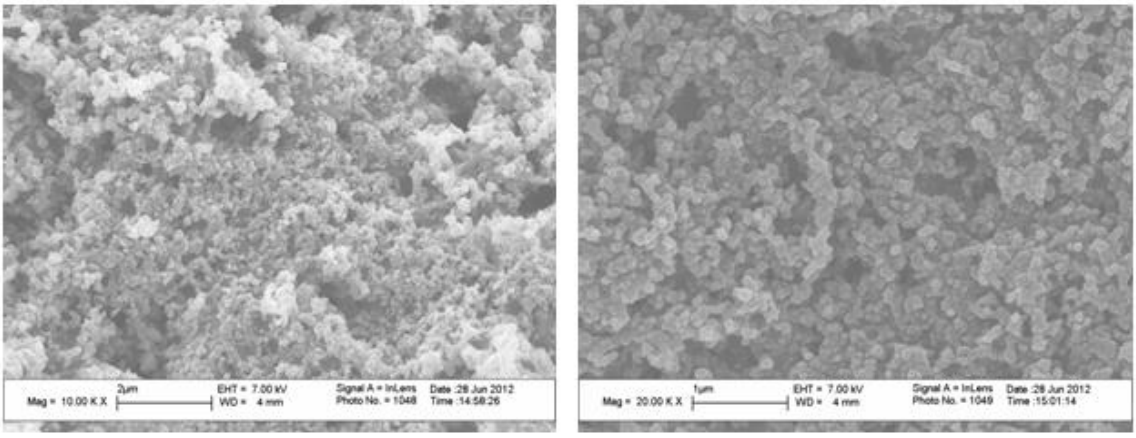

(a) **(b)**

Figure 3-17. SEM images of composite PVBPT (PVBPT – 10%, Filler – 80%, Binder – 10%) sputter coated with platinum.

Chapter IV: Summary and Conclusions

The objectives of this study were to investigate the fabrication, assembly and electrochemical characterization of organic, polymer based Lithium ion batteries. The summary points and conclusion statements from this study are listed below:

- Batteries with Lithium metal and graphite anode, pure and composite PTMA, pure PVBPT, pure and filled PEO were evaluated for electrochemical performance.
- Pure and composite PTMA and PVBPT were evaluated for morphological properties.
- The estimated characteristic scan rate for $LiCoO_2$ is very low compared to organic electrodes.
- From the nyquist plots (absence of second semi circle) and CV plots (high characteristic scan rate), it can be infered that most redox reactions may take place at the interface, while in conventional electrode it is within bulk (Li ion moving inside the channels of the cathode).
- SEM analysis showed a thicker flake-like layer of insulating pure polymer and a uniform particle morphology for composite polymer.
- The EIS data beyond the first semicircle is inconclusive. There appears to be a curvature indicating a semicircle corresponding to charge transfer impedance. Warburg impedance is expected to follow, although not observed in this scan. Further verifications will be required

- Spin coating is generally not suitable for composite polymers.
- Addition of filler has increased the charging capacity of the battery but no apparent improvement in the discharge capacity.
- Inclusion of polymer electrolyte has enabled the making of a flexible battery.
- Conventional battery exhibited both oxidation and reduction peaks where as pure polymer based batteries exhibited only oxidation peak and plain discharging.
- Inclusion of filler has increased the surface film resistance.
- Except for conventional battery all other batteries exhibited charging and discharging all over the applied potential window.

Table 4-1. Summary of CV results.

Battery Label	Cyclic Voltammetry				
	Working Potential (V)	Standard Redox Potential (V vs. vs. Li/Li^+)	Maximum charge and discharge current(mA)		Estimated characteristic scan rate (V/s)
B1 ($LiCoO_2$)	3.6-4.4	3.9	0.87	0.6	10µ
B2 (Pure PTMA)	0-4	0-4	0.06	0.14	10m
B3 (composite PTMA)	0-4	0-4	0.6	2.1	1m
B4 (Pure PVBPT)	0-4	0-4	0.18	0.5	10m
B5 (coin cell with SPE)	0-4	-	0.17	-	-
B6(Flexible cell with 10% filled PEO)	0-4	-	0.44	-	-
B7(Flexible cell with 15% filled PEO)	0-4	-	0.24	-	-

Table 4-2. Summary of Energy and Power results.

Battery Label	Charging and Discharging energy (J)		Energy efficiency (%)	Charging and Discharging Capacity (mAh)		Coulombic efficiency (%)
B1 ($LiCoO_2$)	54644	33134	61	4.3	2.6	60
B2 (Pure PTMA)	44.5	10.7	24	0.0054	0.0025	46
B3 (composite PTMA)	302	80	26	0.029	0.011	38
B4 (Pure PVBPT)	67.2	51.7	77	0.0097	0.0083	85

Table 4-3. Summary of Various Resistances in a Battery.

Battery Label	Electrochemical Impedance Spectroscopy		
	Electrolyte Resistance (Ω)	Surface film Resistance (Ω)	Charge transfer Resistance (Ω)
B1 ($LiCoO_2$)	5.75	41.5	7.5
B2 (Pure PTMA)	11.1	90	53.24
B3 (composite PTMA)	1.72	1500	5600
B4 (Pure PVBPT)	4.73	38.4	24.7

The future work can be focused on the following aspects:

- Utilizing n-type radical polymers as anode in the battery, hence enabling battery more plastic and safer.
- Developing electro active polymers independently at University of Houston in collaboration with polymer chemists.
- Finding carbon fibers that can be coated to enhance the performance of the polymer electrode.
- Resolving the coating and adhesion problems to improve the overall performance of the battery.
- Resolving the discharge issues associated with the polymer based batteries.

- More conclusive EIS plots will be sought in future work to interpret various mechanisms in the battery including bulk, interface, and charge transfer impedances and ion diffusion. Repeatability and statistical confidence of EIS data will also be addressed in future work.
- Researching on novel methods and materials that can decrease the high impedance across the solid electrode-electrolyte interface.

REFERENCES

1. Hiroyuki Nishide, Shigeyuki Iwasa, Yong-Jin Pu, Takeo Suga, Kentaro Nakahara and Masaharu Satoh. (2004). "Organic radical battery: nitroxide polymers as a cathode-active material." Electrochimica Acta 50(2-3): 827-831.
2. Kentaro Nakahara, Kenichi Oyaizu and Hiroyuki Nishide. (2011). "Organic Radical Battery Approaching Practical Use." Chemistry Letters 40(3): 222-227.
3. Jae-Kwang Kim, Gouri Cheruvally, Jou-Hyeon Ahn, Yang-Gon Seo, Doo Seong Choi, Seo-Hwan Lee and Choong Eui Song. (2008). "Organic radical battery with PTMA cathode: Effect of PTMA content on electrochemical properties." Journal of Industrial and Engineering Chemistry 14(3): 371-376.
4. Kentaro Nakahara, Jiro Iriyama, Shigeyuki Iwasa, Masahiro Suguro, Masaharu Satoh and Elton J. Cairns. (2007). "Cell properties for modified PTMA cathodes of organic radical batteries." Journal of Power Sources 165(1): 398-402.
5. Lucienne Bugnon, Colin J. H. Morton, Petr Novak, Jens Vetter and Peter Nesvadba. (2007). "Synthesis of Poly (4-methacryloyloxy-TEMPO) via Group-Transfer Polymerization and Its Evaluation in Organic Radical Battery." Chemistry of Materials 19(11): 2910-2914.
6. Peter Nesvadba, Lucienne Bugnon, Pascal Maire and Petr Novak. (2009). "Synthesis of A Novel Spirobisnitroxide Polymer and its Evaluation in an Organic Radical Battery" Chemistry of Materials 22(3): 783-788.

7. Hiroyuki Nishide, Kenichiroh Koshika and Kenichi Oyaizu. (2009). "Environmentally benign batteries based on organic radical polymers." Pure & Applied Chemistry 81(11): 1961-1970.
8. Sunao Yoshihara, Haruhiko Katsuta, Hiroshi Isozumi, Masanori Kasai, Kenichi Oyaizu. (2010). "Designing current collector/composite electrode interfacial structure of organic radical battery." Journal of Power Sources 196(18): 7806-7811.
9. Kentaro Nakahara, Jiro Iriyama, Shigeyuki Iwasa, Masahiro Suguro, Masaharu Satoh, Elton J. Cairns. (2007). "High-rate capable organic radical cathodes for Lithium rechargeable batteries." Journal of Power Sources 165(2): 870-873.
10. Masahiro Suguro, Shigeyuki Iwasa, Yuki Kusachi, Yukiko Morioka and Kentaro Nakahara. (2007). "Cationic Polymerization of Poly(vinyl ether) Bearing a TEMPO Radical: A New Cathode-Active Material for Organic Radical Batteries." Macromolecular Rapid Communications 28(18-19): 1929-1933.
11. Kentaro Nakahara, Shigeyuki Iwasa, Yukiko Morioka, Jiro Iriyama, Masahiro Suguro and E. Hasegawa. (2002). "Rechargeable batteries with organic radical cathodes." Chemical Physics Letters 359(5-6): 351-354.
12. Takeo Suga, Shuhei Sugita, Hiroki Ohshiro, Kenichi Oyaizu and Hiroyuki Nishide. (2010). "p- and n-Type Bipolar Redox-Active Radical Polymer: Toward Totally Organic Polymer-Based Rechargeable Devices with Variable Configuration." Advanced Materials 23(6): 751-754.

13. Kenichiroh Koshika, Naoki Sano, Kenichi Oyaizu and Hiroyuki Nishide. (2009). "An Aqueous, Electrolyte-Type, Rechargeable Device Utilizing a Hydrophilic Radical Polymer-Cathode." Macromolecular Chemistry and Physics 210(22): 1989-1995.
14. Kenichi Oyaizu, Yuko Ando and Hiroyuki Nishide. (2008). "Nernstian Adsorbate-like Bulk Layer of Organic Radical Polymers for High-Density Charge Storage Purposes." Journal of the American Chemical Society 130(44): 14459-14461.
15. Kenichi Oyaizu, Takeo Suga, Kentaro Yoshimura and Hiroyuki Nishide. (2008). "Synthesis and Characterization of Radical-Bearing Polyethers as an Electrode-Active Material for Organic Secondary Batteries." Macromolecules 41(18): 6646-6652.
16. Sunao Yoshihara, Hiroshi Isozumi, Masanori Kasai, Hisatomo Yonehara, Yuko Ando, Kenichi Oyaizu and Hiroyuki Nishide. "Improving Charge/Discharge Properties of Radical Polymer Electrodes Influenced Strongly by Current Collector/Carbon Fiber Interface." The Journal of Physical Chemistry B 114(25): 8335-8340.
17. Ali A. Golriz, Tassilo Kaule, Jeanine Heller, Maria B. Untch, Phillip Schattling, Patrick Theato, Masaya Toda, Shinya Yoshida, Takahito Ono, Hans-Jurgen Butt, Jochen Stefan Gutmann and Rudiger Berger. (2011). "Redox active polymers with phenothiazine moieties for nanoscale patterning via conductive scanning force microscopy." Nanoscale 3(12): 5049-5058.
18. Hiroyuki Nishide and Takeo Suga. (2005). “Organic Radical Battery.” The Electrochemical Society Interface.

19. Daniel A. Scherson and Attila Palencsár. (2006). “Batteries and Electrochemical Capacitors.” The Electrochemical Society.
20. Vincent, C. A. (2000). "Lithium batteries: a 50-year perspective, 1959-2009." Solid State Ionics 134(2000): 159-167.
21. Riccardo Ruffo, Colin Wessells, Robert A. Huggins, Yi Cui. (2009). "Electrochemical behavior of LiCoO2 as aqueous Lithium-ion battery electrodes." Electrochemistry Communications 11(2): 247-249.
22. Tarascon, J. M. and M. Armand (2001). "Issues and challenges facing rechargeable Lithium batteries." Nature 414(6861): 359-367.
23. Oyaizu, K. and H. Nishide (2009). "Radical Polymers for Organic Electronic Devices: A Radical Departure from Conjugated Polymers?" Advanced Materials 21(22): 2339-2344.
24. MECE 7397- Material for Energy Storage Class, University of Houston, spring 2011, Haleh Ardebili.
25. Jishi Zhao, Li Wang, Xiangming He, Chunrong Wan and Changyin Jiang. (2010). "Kinetic Investigation of LiCoO2 by Electrochemical Impedance Spectroscopy (EIS)." Int. J. Electrochem. Sci., 5 (2010) 478 - 488.
26. Pallavi Verma, Pascal Maire and Petr Novak. “A review of the features and analyses of the solid electrolyte interphase in Li-ion batteries.” Electrochimica Acta 55(22):6332-6341.
27. Shiro Seki, Yo Kobayashi, Hajime Miyashiro, Atsushi Yamanaka, Yuichi Mita, Toru Iwahori. (2005). “Degradation mechanism analysis of all-solid-state Lithium

polymer secondary batteries by using the impedance measurement." Journal of Power Sources, Volume 146, Issues 1–2, Pages 741-744, ISSN 0378-7753.

28. S.S. Zhang, K. Xu and T.R. Jow. (2006). "EIS study on the formation of solid electrolyte interface in Li-ion battery." Electrochimica Acta, Volume 51, Issues 8–9, Pages 1636-1640, ISSN 0013-4686.
29. K. Hanai, M. Ueno, N. Imanishi, A. Hirano, O. Yamamoto and Y. Takeda. (2011). "Interfacial resistance of the LiFePO4-C/PEO-LiTFSI composite electrode for dry-polymer Lithium-ion batteries." Journal of Power Sources, Volume 196, Issue 16, Pages 6756-6761, ISSN 0378-7753.
30. P.L. Moss, G. Au, E.J. Plichta and J.P. Zheng. "Investigation of solid electrolyte interfacial layer development during continuous cycling using ac impedance spectra and micro-structural analysis." Journal of Power Sources, Volume 189, Issue 1, Pages 66-71, ISSN 0378-7753.
31. Yanliang Liang, Zhanliang Tao and Jun Chen. "Organic Electrode Materials for Rechargeable Lithium Batteries." Advanced Energy Materials 2(7):742-769.